

SHOCK PROPAGATION IN A TARGET SUBJECTED TO HYPERVELOCITY IMPACT OF AN INCIDENT PROJECTILE

by T. Fu

**CASE FILE
COPY**

April 1970

SCIENCE & ENGINEERING



BROWN ENGINEERING

A TELEDYNE COMPANY

Research Park • Huntsville, Alabama 35807

TECHNICAL NOTE
SE-289

SHOCK PROPAGATION IN A TARGET SUBJECTED TO
HYPERVELOCITY IMPACT OF AN INCIDENT PROJECTILE

By
T. Fu, Ph. D.

April 1970

Prepared For

SPACE SCIENCES LABORATORY
GEORGE C. MARSHALL SPACE FLIGHT CENTER
HUNTSVILLE, ALABAMA

Contract No. NAS8-20166


Prepared By

SPACE AND MILITARY SYSTEMS DIVISION
SCIENCE AND ENGINEERING GROUP
BROWN ENGINEERING COMPANY, INC.
HUNTSVILLE, ALABAMA


ABSTRACT

A hydrodynamic model, based on shock diffraction theory and the quasi-similarity solutions of blast wave theory, is developed to describe the shock profile history in a metal target on which a hyper-velocity metal projectile impacts. A finite difference integration of the resultant method of characteristic solution is used to obtain numerical results. A numerical example of aluminum impacting on aluminum at a velocity of 20 km/sec is presented. The comparison with the direct numerical results shows a good agreement for the case selected.

Approved:


Harry C. Crews, Jr.
Manager
Space and Military Systems Division

Approved:


J. E. White, Jr.
Program Manager
Science and Engineering Group

Approved:

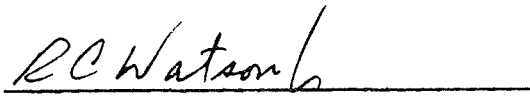

R. C. Watson, Jr.
Vice President
Science and Engineering Group

TABLE OF CONTENTS

	Page
INTRODUCTION.	1
THEORETICAL MODEL OF IMPACT-GENERATED SHOCK PROPAGATION IN SOLID MEDIA	4
FORMULATION OF THE CHARACTERISTIC EQUATIONS .	8
Two-Dimensional Case	8
Axisymmetric Cases	16
HUGONIOT RELATIONS OF SHOCK WAVES IN SOLID MEDIA	20
c, s Materials	20
Aluminum	22
SHOCK PROPAGATION LAWS	25
SHOCK WAVE INTERACTION WITH FREE BOUNDARY . .	29
CONSTRUCTION OF NUMERICAL SOLUTIONS FOR SHOCK WAVE PROPAGATIONS	32
Initial Normal Shock Waves	32
Simple Wave Solutions.	34
Asymptotic Solution of Two-Dimensional Shock Profiles for Strong Shock.	36
Finite Difference Solutions to the Characteristic Equations	37
AN APPROXIMATION FOR PRESSURE PULSE AT LATE STAGE OF IMPACT	40
NUMERICAL RESULTS AND DISCUSSION	46
The Starting Point of Shock Curvature	46
The Successive Positions of Shock Profiles	48
Pressure Distribution.	50

TABLE OF CONTENTS - Concluded

	Page
SUMMARY	53
APPENDIX. SOUND SPEED OF c , s MATERIAL BEHIND THE SHOCK	54
REFERENCES	58

LIST OF ILLUSTRATIONS

Figure	Title	Page
1	General Features of the Hypervelocity Impact Mechanism	5
2	Moving Shock Front in a Suddenly Enlarged Channel.	6
3	"Ray Tube" Coordinate System	9
4	Geometric Relation of Equations 2 and 3 for Two-Dimensional Case	9
5	"Mach Angle" in Physical Plane	13
6	Relations of (x, y) Plane and (β , t) Plane .	13
7	Sketch of Shock Propagation in Solid Medium	14
8	Intrinsic Coordinate System of Axisymmetric Case	17
9	Geometric Relation for Axisymmetric Cases	17
10	The Ratio of Adiabatic Sound Speed and the Scope of Rankine-Hugoniot Curve as a Function of Shock Mach Number for c, s Material . .	23
11	Shock Wave and Free Surface Interaction. .	30
12	Impact-Generated Normal Shock Waves . .	33
13	Construction of a Simple Wave Solution . .	35
14	Approximate Shock Profile for the Strong Shock Situation (U Large).	38

LIST OF ILLUSTRATIONS - Concluded

Figure	Title	Page
15	Spherical Coordinate System With Symmetric Axis	42
16	The Starting Point of Shock Curvature in Aluminum	47
17	Successive Shock Profiles for Aluminum-on- Aluminum Impact	49
18	Comparison of Peak Pressure Distribution for Aluminum-on-Aluminum Impact	51
19	Angular Pressure Distribution	52

LIST OF SYMBOLS

A	Shock front area
A'	dA/dU
a	Adiabatic sound speed
a_1, a_2, a_3	Shock relation coefficients in Equation 34
b_1, b_2, b_3	Shock relation coefficients in Equation 35
C	Equivalent "sound speed" in Equation 9
C_{\pm}	Physical characteristics
c	Dilatational wave speed
e	Specific internal energy
f	Dimensionless velocity
g	Dimensionless pressure
h	Dimensionless density
ℓ	Length measured along the shock front
ℓ_{\pm}	Riemann invariants
m	Equivalent "Mach angle" in Equation 15
p	Pressure
R	Shock position
r	Radial position from symmetric axis
S	Entropy
s	Material constant
T	Temperature
t	Time

t_c	Characteristics time; $t \geq t_c$ normal shock portion vanishes
U	Shock velocity
u	Particle velocity
x, y	Two-dimensional Cartesian coordinates
z	Cylindrical coordinate
β	"Ray" coordinate; shock inclination angle
Γ	Grüneisen ratio
Γ_{\pm}	Holograph characteristics
ξ	Similarity variable, $\xi = r/R$
ρ	Density
μ	Area function defined in Equation 41
θ	Shock angle
λ	Shock decay factor in Equation 58
ω	Prandtl-Meyer function

INTRODUCTION

In order to protect a space vehicle against meteoroid hazards, it is necessary to understand the meteoroid impact phenomena and the penetration mechanism. The meteoric particles, in spite of generally being small in size, possess high kinetic energies because of their hypervelocity nature (ranging from 11 km/sec to 72 km/sec). Generally speaking, the term "hypervelocity impact" is defined as the collision of two solid bodies with a relative velocity higher than the elastic wave propagation speed in the material under consideration.

The impact mechanisms are governed by an extremely complex system of nonlinear, partial differential equations with very complicated boundary conditions. To solve this problem analytically is a rather formidable task. Since 1958, several computer programs (Refs. 1 through 6) have been developed which permit complete solutions through direct numerical analysis. A survey of this subject reveals that not only a tremendous amount of computing time is required for operating these computer programs, but large errors may develop because of the numerical fluctuations inherent in such solutions. In spite of these deficiencies, the numerical method is still considered the principal approach to obtaining a complete solution of hypervelocity impact.

In addition to the numerical solutions obtained by the huge computer programs, analytic solutions of hypervelocity impact have been obtained by many authors. An excellent review of such solutions has been given by Rae (Ref. 7). So-called "analytic treatments" of hypervelocity impact usually refer to those approximate solutions which, even though yielding less exact results than the numerical methods, are easily obtained and, most importantly, still display the essential features of the problem. Since solutions cannot be obtained in a rigorous manner by the available analytic techniques without considerable simplifications, clearly each approximate method is valid only for the conditions for which the simplifying assumptions apply.

Blast wave theory (Refs. 7 and 8), for instance, yields shock profiles in good agreement with direct numerical solutions at a late stage of impact, e. g., an appreciable period of time after impact. The blast wave solutions, however, are not applicable to the thin target plate since the thickness of the target is comparable to the projectile dimensions which invalidates point source assumption. The blast wave solution, however, does reveal the important fact that there exists a close analogy between the propagation of shocks for a thick target resulting from explosions and those resulting from hypervelocity impact.

In the present study, a cylindrical projectile impacting on a target of infinite depth is considered. At the instant of impact, a plane shock is generated on the target surface with the shock area equal to the circular cross section of the incident primary cylinder. Consideration is then directed to describing the shock profiles as time elapses. The initial conditions are considered to be equivalent to a surface explosion of finite area on the target surface, an equivalence which has also been used by Zeldovich (Ref. 9), among other Soviet scientists, as the idealized model which describes the initial stage of impact. He did not, however, actually calculate the subsequent shock profiles as functions of time. The formulations of the shock profiles in the present study are based on a shock dynamic theory (Refs. 10 and 11) in fluid mechanics. The two-dimensional method of characteristics is employed to calculate the successive positions of shock waves as a function of time. The equations of state for metals are used in the formulation, and the shock interaction with the free boundary is also considered.

The major shortcoming of this theoretical model is that it yields no information on the properties far behind the shock wave except immediately at the shock as deduced from Hugoniot relations. Because the shock wave develops in a hemispherical shape in a short period after impact, quasi-similar solutions of blast wave theory (Ref. 12) are used to approximate the fluid functions in the region behind the shock wave.

The object of this study is to calculate the shock profiles resulting from hypervelocity impact and to use these results in predicting the impact phenomena such as crater formation and spallation fractures. The applications of shock propagations in solid medium will be reported later.

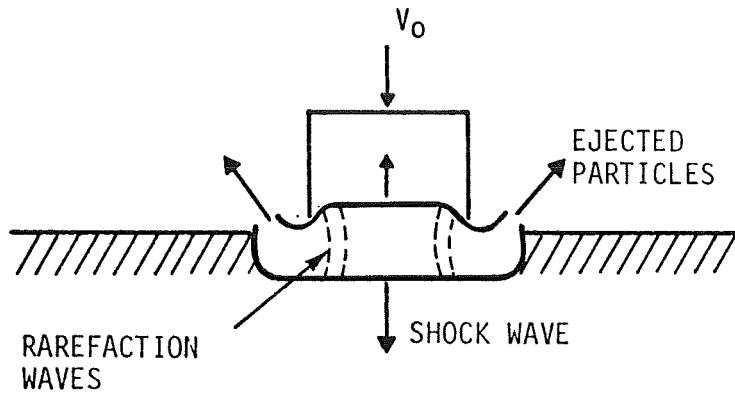
A numerical example is given in this report and compared with the existing results of other investigations. The agreement in general is good.

The author wishes to express his appreciation to Mr. Carl Young for his discussions of the problem; and Dr. G. R. Guinn for his guidance and encouragement during the course of this work.

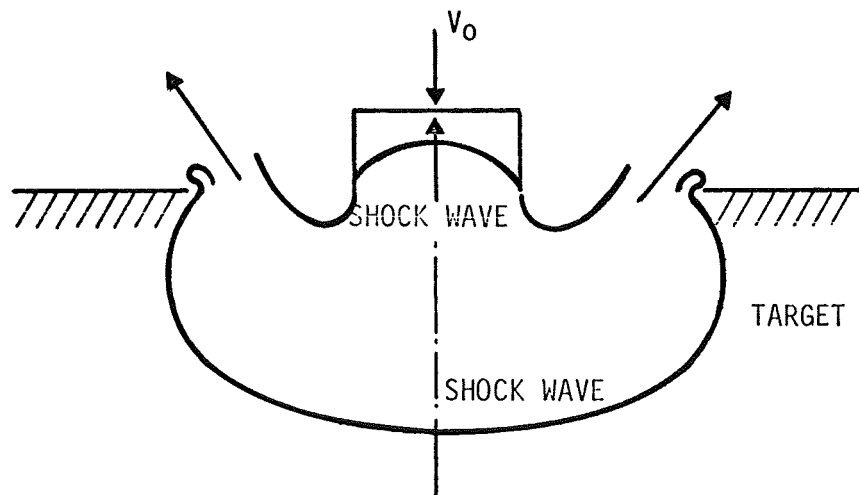
THEORETICAL MODEL OF IMPACT-GENERATED SHOCK PROPAGATION IN SOLID MEDIA

The physical features of hypervelocity impact can be illustrated schematically in Figure 1, in which a cylindrical projectile traveling at a high velocity is assumed to strike a semi-infinite target. Immediately after the impact (Figure 1a) there are two strong shock waves moving in opposite directions: one traveling forward into the target and the other backward into the projectile. The pressures generated by the impact are so high in the material through which the shock has passed that the material strength is comparatively negligible. Therefore the material behind the shock wave is considered to behave essentially as an inviscid, compressible fluid. As the shock wave advanced further into the target material, the plane portion of the shock wave is gradually "consumed" by the rarefaction waves from the corners (see Figure 1b). The shock front becomes distorted and attenuated in strength, and eventually approaches the shape of a hemisphere. After an extended elapsed period of time after impact, the crater is formed in the target (Figure 1c). Further advancement into the semi-infinite target will cause the shock wave to degenerate into the plastic waves and then into the elastic wave.

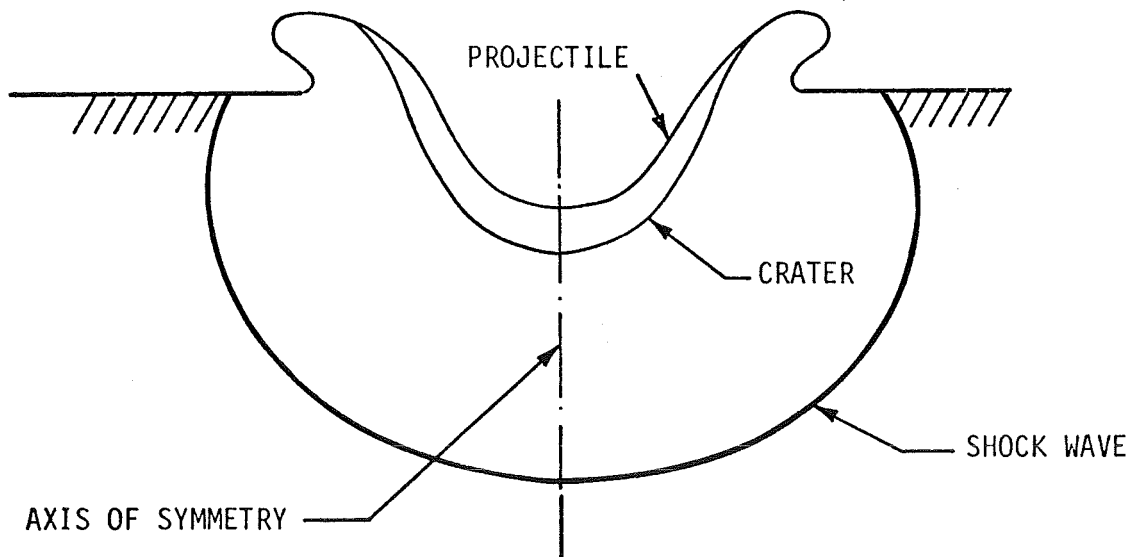
The geometric development of the impact shock, in an idealized sense, resembles a moving shock in unsteady, supersonic flow. Figure 2 illustrates a normal shock moving along a channel whose wall is suddenly enlarged and, as a result of the enlargement, the shock wave changes its shape as it propagates into the enlarged area with subsequent diminishing of the plane shock by the rarefaction wave issuing from the corner of the wall. The mathematical formulation of this problem will be given in the next two sections.



(a) Brief Elapsed Time After Impact



(b) Intermediate Elapsed Time After Impact



(c) Extended Period of Time After Impact

FIGURE 1. GENERAL FEATURES OF THE HYPERVELOCITY IMPACT MECHANISM

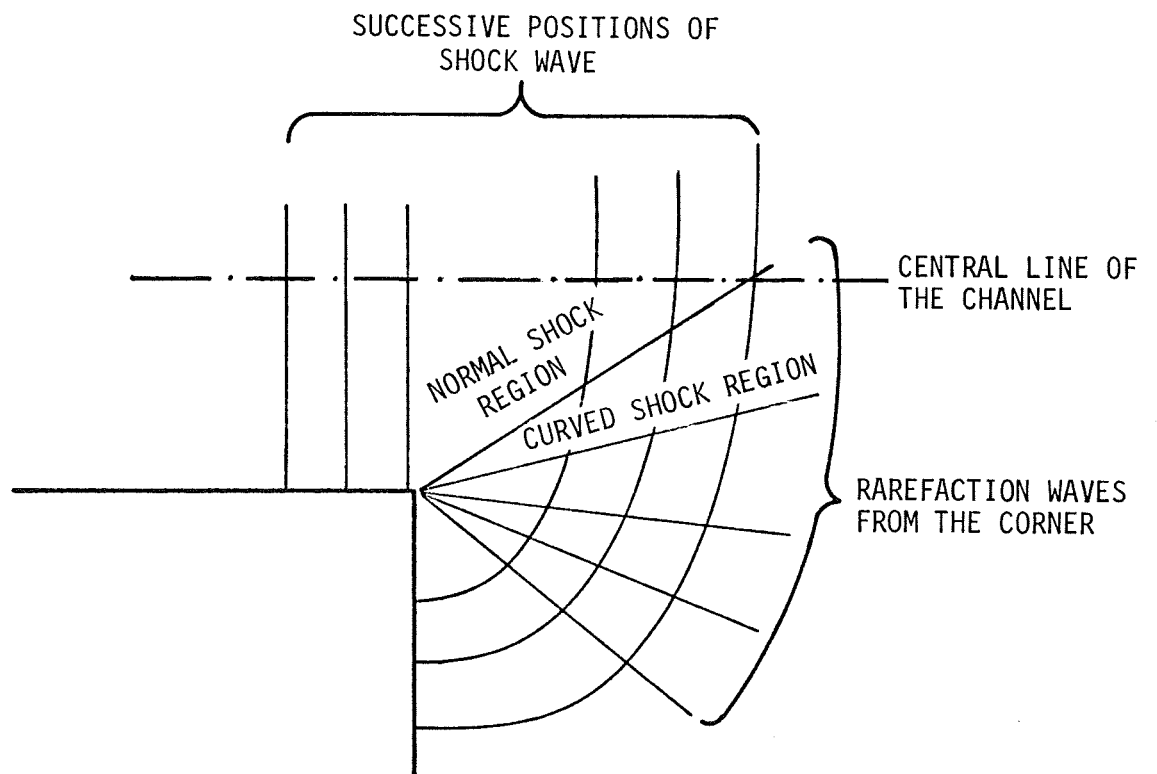


FIGURE 2. MOVING SHOCK FRONT IN A SUDDENLY ENLARGED CHANNEL

Figure 1a also illustrates the manner in which the material particles are splashed upward from the free boundary of the target, and the shock wave's interaction with the target surface. The interaction between shock waves and the free surface should be considered as the boundary condition in the calculation of shock profiles as will be described later.

FORMULATION OF THE CHARACTERISTIC EQUATIONS

The mathematical formulation of the shock profile relationships are based on a shock dynamics theory suggested by Whitham (Ref. 13) for plane shock with a corner. In the present study, the two-dimensional computational scheme is essentially the same as that of Skews (Ref. 10), while the formulation of axisymmetric case follows a recent paper of Hayes (Ref. 11). It should be noted that the formulations of this section only apply to a region away from the free surface of the target. In the neighborhood of the free surface, shock waves and free surface interaction are considered separately in a subsequent section.

TWO-DIMENSIONAL CASE

In Figure 3, an orthogonal coordinate system (β , t) is constructed to describe the motion of shock waves, where t corresponds to the successive instants of shock wave history and β is called "ray" to describe a specific portion of the shock wave. A basic assumption is that each small portion of the shock, which is bounded by a "ray-tube", may be treated independently as one-dimensional flow and obeys the shock propagation law. The shock propagation law is a relation between the ray tube area A and the shock velocity U :

$$A = A(U) \quad (1)$$

which will be derived in a later section.

In the physical plane (Figure 4), the arc lengths \overline{PQ} and \overline{PS} are defined as

$$\overline{PQ} = U dt$$

$$\overline{PS} = A d\beta .$$

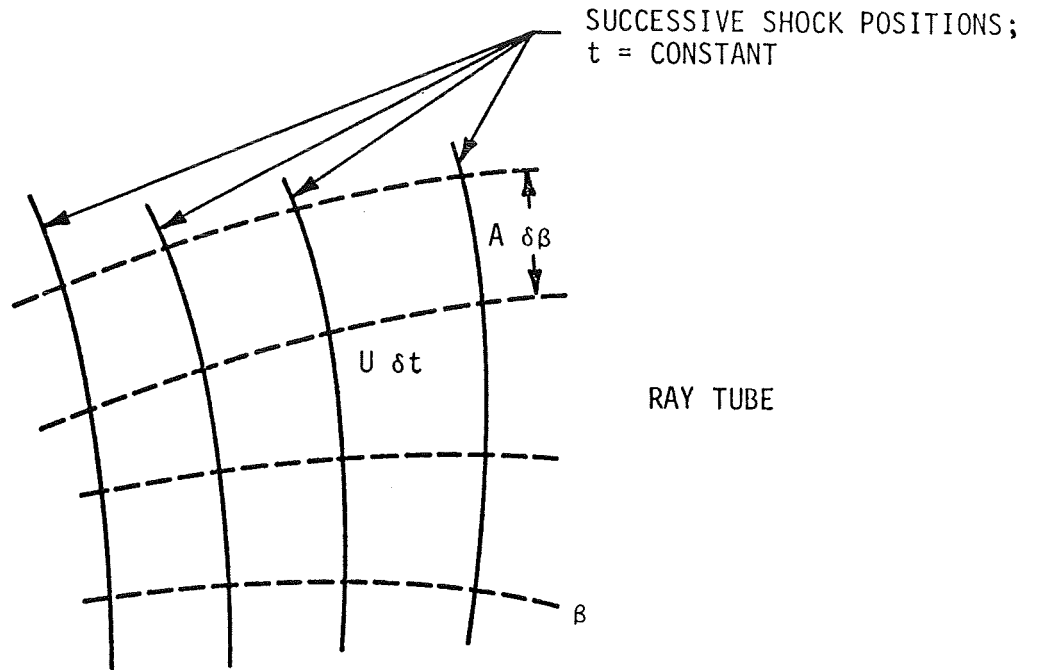


FIGURE 3. "RAY TUBE" COORDINATE SYSTEM

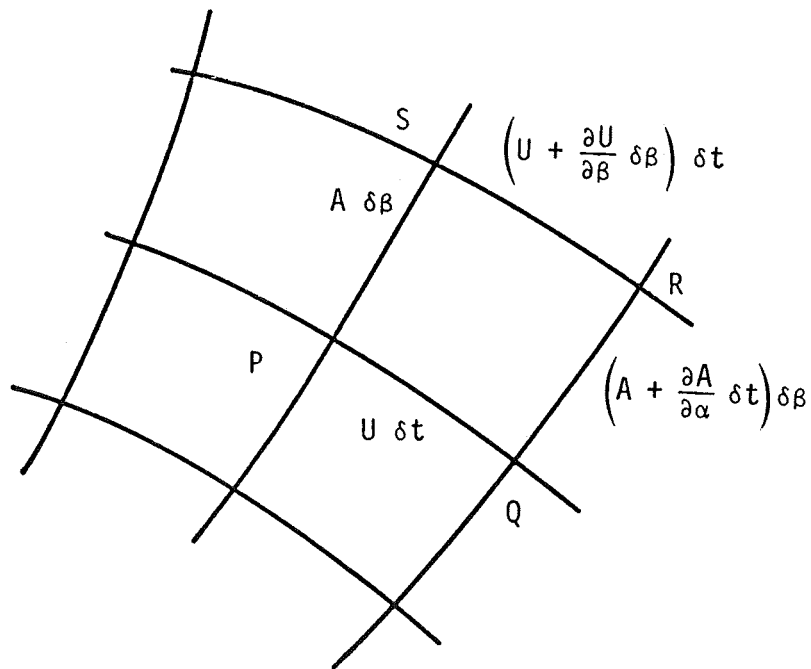


FIGURE 4. GEOMETRIC RELATION OF EQUATIONS 2 AND 3 FOR TWO-DIMENSIONAL CASE

Let $\theta(\beta, t)$ be the angle between the ray and a fixed direction.
Then the change of θ from P to S is

$$\delta\theta = \frac{\overline{QR} - \overline{PS}}{\overline{PQ}} = \frac{1}{U} \cdot \frac{\partial A}{\partial t} \cdot \delta\beta$$

or

$$\frac{\partial\theta}{\partial\beta} - \frac{1}{U} \cdot \frac{\partial A}{\partial t} = 0 \quad . \quad (2)$$

Similarly,

$$-\delta\theta = \frac{\overline{SR} - \overline{PQ}}{\overline{PS}} = \frac{1}{A} \cdot \frac{\partial U}{\partial\beta} \delta t$$

or

$$\frac{\partial\theta}{\partial t} + \frac{1}{A} \cdot \frac{\partial U}{\partial\beta} = 0 \quad . \quad (3)$$

Notice that the derivations above are obtained from purely geometrical reasoning. A combination of Equations 2 and 3 indicates the kinematic relation between U and A:

$$\frac{\partial}{\partial t} \left(\frac{1}{U} \cdot \frac{\partial A}{\partial t} \right) + \frac{\partial}{\partial\beta} \left(\frac{1}{A} \frac{\partial U}{\partial\beta} \right) = 0 \quad . \quad (4)$$

When Equation 1 is combined with Equation 4, the shock positions are determined for all times. The kinematic relations may be written in terms of U as follows:

$$\frac{\partial\theta}{\partial\beta} - \frac{A'(U)}{U} \cdot \frac{\partial U}{\partial t} = 0 \quad (5)$$

$$\frac{\partial \theta}{\partial t} + \frac{1}{A(U)} \cdot \frac{dU}{d\beta} = 0 \quad (6)$$

or equivalently,

$$\frac{\partial}{\partial t} \left(\frac{A'(U)}{U} \cdot \frac{\partial U}{\partial t} \right) + \frac{\partial}{\partial \beta} \left(\frac{1}{A(U)} \cdot \frac{\partial U}{\partial \beta} \right) = 0 \quad (7)$$

where $A'(U) = \frac{dA(U)}{dU}$.

The above equations are analogous to the equations of non-linear sound waves or two-dimensional steady supersonic flows; hence the existing theories of compressible fluid flows on these topics can be equivalently applied to the present problems.

By the theory of characteristics, Equations 5 and 6 yield

$$\left(\frac{\partial}{\partial t} \pm C \frac{\partial}{\partial \beta} \right) \left(\theta \pm \int \frac{dU}{AC} \right) = 0 \quad (8)$$

where C is the equivalent "sound speed":

$$C = \left[\frac{-U}{A(U) A'(U)} \right]^{\frac{1}{2}} \quad (9)$$

Let ℓ_+ , ℓ_- be the Riemann invariants of characteristics C_+ and C_- , respectively. Then Equation 8 gives

$$C_+; \quad \theta + \omega(U) = \ell_+ \quad \text{on} \quad \frac{d\beta}{dt} = +C \quad (10)$$

$$C_-; \quad \theta - \omega(U) = \ell_- \quad \text{on} \quad \frac{d\beta}{dt} = -C \quad (11)$$

and

$$\omega(U) = \int \frac{dU}{AC} \quad (12)$$

Let $m(\alpha, \beta)$ be the angle between a characteristic and a ray (see Figure 5). The characteristic lines have the direction

$$\frac{dy}{dx} = \tan (\theta \pm m) \quad (13)$$

on the physical plane. The positive sign in Equation 13 corresponds to left-running characteristics and the negative sign to right-running characteristics; m is equivalent to the "Mach angle" in two-dimensional steady flows.

Figure 6 shows that the increment \overline{PR} along a left-running characteristic can be related to dt and $d\beta$ in the (β, t) plane by

$$dx = U dt \cos (\theta + m) / (\cos m)$$

$$dy = U dt \sin (\theta + m) / (\cos m)$$

$$\text{or} \quad (14)$$

$$dx = A d\beta \cos (\theta + m) / (\sin m)$$

$$dy = A d\beta \sin (\theta + m) / (\sin m)$$

and

$$\tan m = \frac{A}{U} \cdot \frac{d\beta}{dt} = \frac{AC}{U} \quad (15)$$

Similar relations can be found for right-running characteristics by simply changing $\theta + m$ to $\theta - m$ in Equation 14.

Figure 7 shows that a plane shock, starting at the edge of a solid medium enters a sudden enlargement area at time $t = 0$. For $t > 0$, there are two central fans emitted from the "corners", which cause the shock

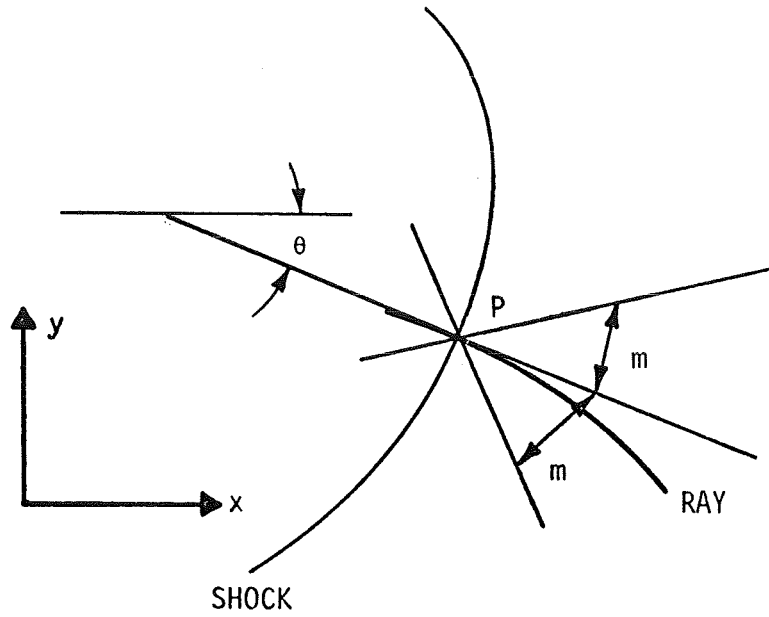


FIGURE 5. "MACH ANGLE" IN PHYSICAL PLANE

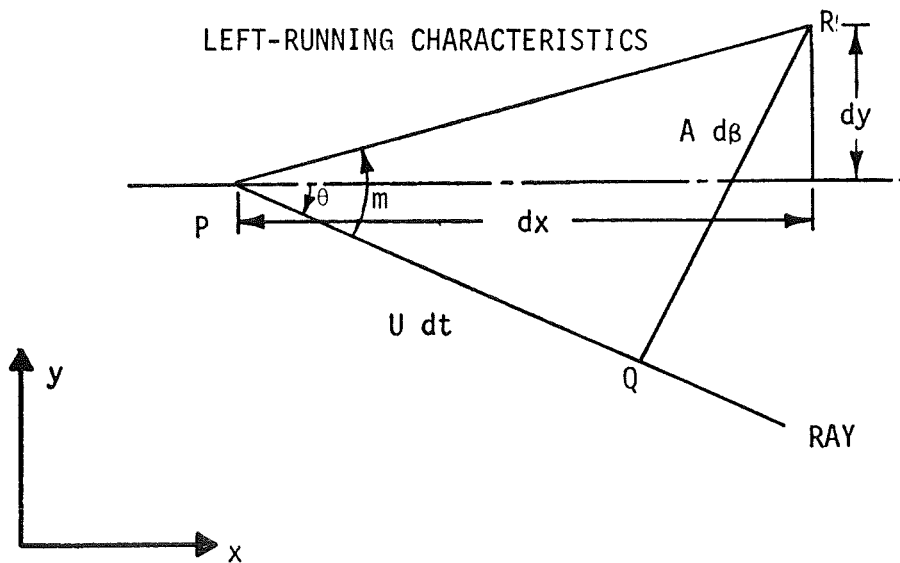
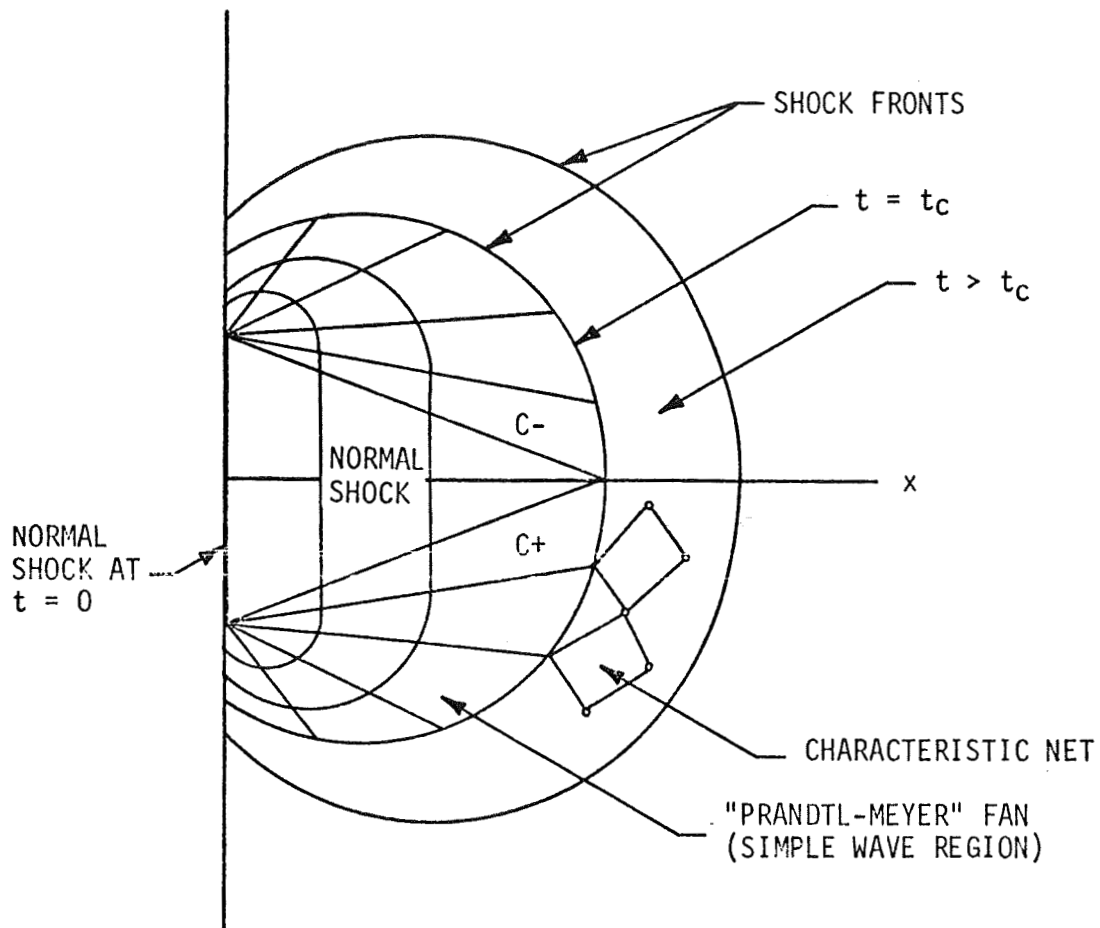


FIGURE 6. RELATION OF (x, y) PLANE AND (β, t) PLANE



- NOTES: 1. t_c is the time when the first characteristic reaches the shock centerline (x -axis).
2. The normal shock portion vanishes completely for $t \geq t_c$.

FIGURE 7. SKETCH OF SHOCK PROPAGATION IN SOLID MEDIUM

front to expand. The normal shock portion is therefore diminishing in the course of time. Before the time t_c (defined in Figure 7), the physical picture is a simple wave pattern. Therefore U , θ , m are invariants along a characteristic line. Direct integration of Equation 14 yields

$$\begin{aligned}x/t &= U \cos (\theta + m) / \cos m + x_0/t \\y/t &= U \sin (\theta + m) / \cos m + y_0/t \\x/\beta &= A \cos (\theta + m) / \sin m + x_0/\beta \\y/\beta &= A \sin (\theta + m) / \cos m + y_0/\alpha\end{aligned}\tag{16}$$

where (x_0, y_0) is the initial point. Similarly, changing m to $-m$ in Equation 16 gives the integrated equation for right-running characteristics.

When $t > t_c$, the simple wave theory ceases to apply and the shock profiles can be predicted only by constructing the characteristic nets, in the same manner as a two-dimensional nozzle flow field.

The simple wave solution of two-dimensional cases is only hypothetical, since the shock waves generated by the projectile of finite dimensions are three-dimensional. The axisymmetric case is the simplest three-dimensional flow configuration.

In the next subsection, similar treatment will be given for axisymmetric impact problems. A finite difference numerical scheme is adopted because of the nonexistence of simple wave solutions. To do so, a starting line should be chosen to construct the net of characteristic lines.* The solutions on the starting line are the simple wave solutions described in this subsection.

*In steady, axisymmetric supersonic flow calculations at the exit of a nozzle, the Prandtl-Meyer expansion fan, which is a simple wave solution, is used to provide such a starting line (Ref. 14).

AXISYMMETRIC CASES

As mentioned previously, the characteristic equations for axisymmetric shock propagation can be formulated in a similar way as in two-dimensional case, except that the basic coordinate system (β, t) must be redefined.

To construct the axisymmetric solutions, the basic coordinate system (β, t) is defined such that the distance along a ray between the shock positions given by t and $t + dt$ is $U dt$, and that $A d\beta/r$ is the distance between the ray β and $\beta + d\beta$; r is the distance from the axis of symmetry and U is the shock velocity (see Figure 8).

Let $\theta(\beta, t)$ be the angle between the ray and the axis of symmetry. The change of θ from P to S (see Figure 9) is

$$\delta\theta = \frac{\overline{RQ} - \overline{PS}}{\overline{PQ}} = \frac{1}{U} \cdot \frac{\partial}{\partial t} \frac{A}{r} \delta\beta$$

or

$$\frac{\partial\theta}{\partial\beta} - \frac{1}{Ur} \frac{\partial A}{\partial t} + \frac{A}{r^2} \cdot \sin\theta = 0 \quad (17)$$

where the relation $(U \partial t)/\partial r = \sin\theta$ is used and $\theta = 0$ at the axis of symmetry.

A similar treatment for the change of θ from P to Q gives

$$\frac{\partial\theta}{\partial t} + \frac{r}{A} \cdot \frac{\partial U}{\partial\beta} = 0 \quad (18)$$

Let $\delta l = A \delta\beta/r$ be the distance between the rays β and $\beta + \delta\beta$. Equations 17 and 18 then become

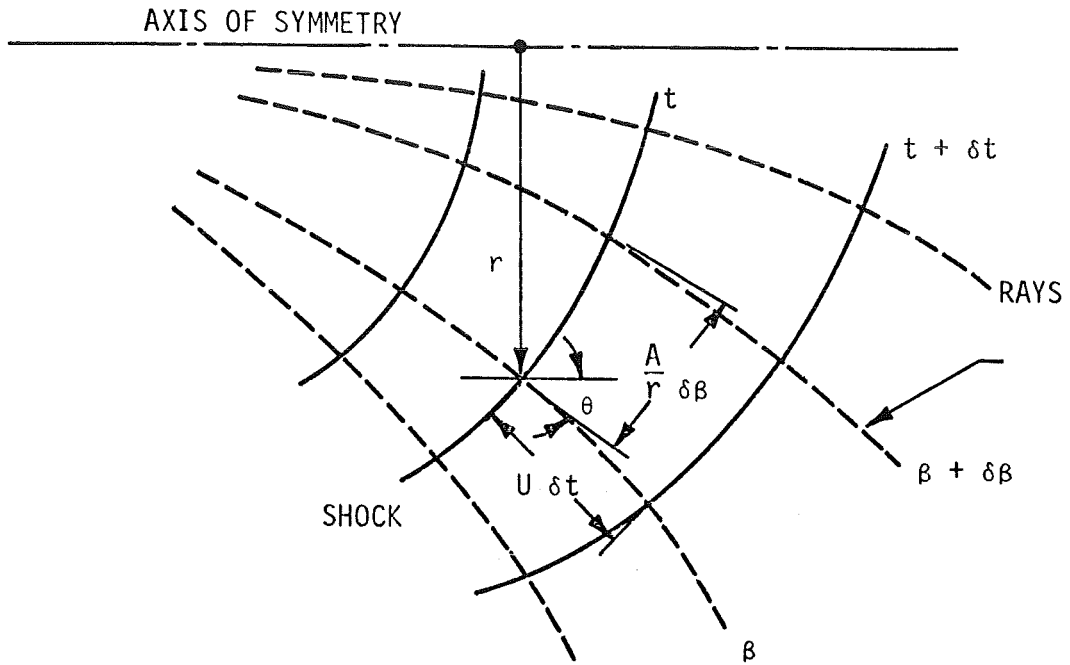


FIGURE 8. INTRINSIC COORDINATE SYSTEM OF AXISYMMETRIC CASE

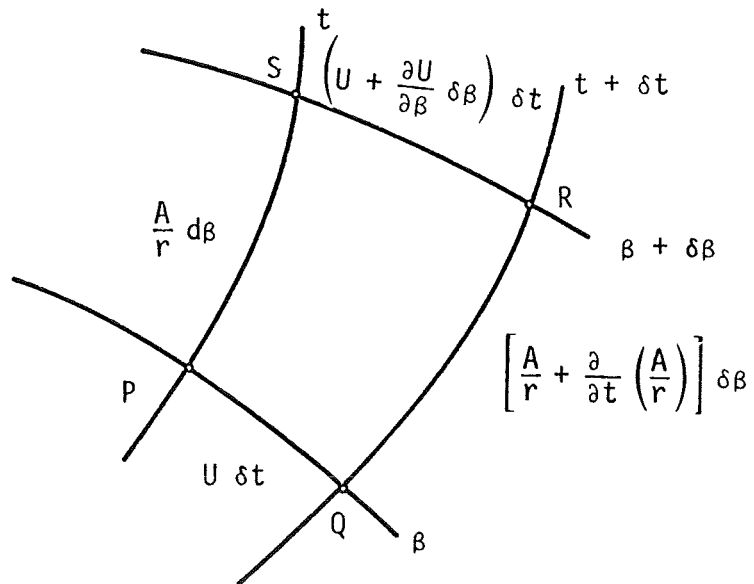


FIGURE 9. GEOMETRIC RELATION FOR AXISYMMETRIC CASES

$$\frac{\partial \theta}{\partial \ell} - \frac{1}{A} \cdot \frac{\partial A}{U \partial t} + \frac{\sin \theta}{r} = 0 \quad (19)$$

and

$$\frac{\partial \theta}{U \partial t} + \frac{\partial U}{U \partial \ell} = 0 \quad (20)$$

Assume that the shock propagation law, i.e., the shock speed and area relation, is expressed in the form (see page 41)

$$\frac{dA}{A} = -\frac{1}{\mu^2} \cdot \frac{dU}{U}$$

where

$$\mu = \mu(U) .$$

Equation 19, then, can be rewritten as

$$\frac{\partial \theta}{\partial \ell} + \frac{1}{\mu^2} \cdot \frac{\partial U}{U^2 \partial t} + \frac{\sin \theta}{r} = 0 \quad (21)$$

Applying the theory of characteristics in Equations 20 and 21 yields

$$\Gamma_{\pm} : \frac{dU}{\mu U} \pm d\theta + \mu \frac{\sin \theta}{r} U dt = 0 \quad (22)$$

along

$$C_{\pm} : \frac{d\ell}{U dt} = \pm \mu \quad (23)$$

where Γ_{\pm} is the compatibility equation of the physical characteristics C_{\pm} .

For a given initial shock shape, the shock shape at later time can be obtained by constructing a finite difference net in the same manner as that of a steady supersonic jet downstream of the nozzle exit section.

Two boundary conditions must be imposed. One is simply that

$$\theta = 0 \quad \text{at} \quad r = 0 .$$

The other condition is on the free boundary where the shock wave interacts the free boundary. The interaction will be described in a later section.

HUGONIOT RELATIONS OF SHOCK WAVES IN SOLID MEDIA

When a shock wave moves into a stationary medium, the flow variables across a shock are governed by the following laws:

- Conservation of mass

$$\rho_0 U = \rho (U - u) \quad (24)$$

- Conservation of momentum

$$p - p_0 = \rho_0 U u \quad (25)$$

- Conservation of energy

$$e - e_0 = \frac{1}{2} (p_0 + p) \left(\frac{1}{\rho_0} - \frac{1}{\rho} \right) \quad (26)$$

where U , u , ρ , p , and e are the shock velocity, fluid velocity, density, pressure, and the specific internal energy of the fluid, respectively. Subscript 0 refers to the undisturbed (or stationary) region.

One more relation is needed to solve the flow across a shock, i.e., the state equation of the material

$$e = f(p, \rho) \quad (27)$$

Recently, many studies have been conducted (Refs. 15, 16, and 17) on the state equation of solid material. So far, no simple and general equation has been formulated. For the sake of convenience, an equation, which relates the shock velocity and the particle velocity u , is used in this work. In general, there are two forms: one applies to so called "c, s material"; the other applies to aluminum.

c, s MATERIALS

In Reference 16, McQueen, et al, use a linear equation

$$U = c + s u \quad (28)$$

which relates the velocities U , u for most metals. c is the dilatational wave speed and s is a constant which is tabulated for 16 materials in their paper. The materials which obey Equation 28 are classified as "c, s materials".

Substituting Equation 28 into Equations 24, 25, and 26, the flow variables are obtained:

$$U = (U - c)/s \quad , \quad (29)$$

$$\rho = \frac{s U}{(s - 1) U + c} \rho_0 \quad , \quad (30)$$

and

$$\rho = \frac{U (U - c)}{s} \rho_0 \quad . \quad (31)$$

The slopes of the Rankine-Hugoniot curve, c_{C-H} , in the (p, ρ) plane is given by

$$c_{C-H}^2 = \frac{c^2}{s^2} (2 M_s - 1) [(s - 1) M_s + 1]^2 \quad (32)$$

where $M_s = U/c$ is the shock Mach number. c_{C-H} differs slightly from the adiabatic sound speed as M_s nears 1, but appreciable discrepancy is found for large shock Mach numbers.

The adiabatic sound speed, $a = (\partial p / \partial \rho)_s$, should be derived by an isentropic process which requires the explicit form of the state equation, Equation 27. But for c, s material, the adiabatic sound

speed, a , can be obtained approximately in terms of the material constants c and s . The resultant expression is

$$a^2 = \frac{c_{C-H}^2}{s^2} [(3s - 1)(s - 1) M_s^2 - 2(s^2 - 3s + 1) M_s - (2s - 1)] . \quad (33)$$

A detailed derivation is given in the Appendix, and a comparison of a and c_{R-H} is made in Figure 10.

It is of interest to point out that the c , s material is very similar to a perfect gas. The range of s varies from 1.2 to 1.9 for most metals, which is analogous to the specific heat ratio of gases. But, it should be stressed that the c , s relation is only an empirical equation. Its accuracy is highly questionable when the shock pressure is greater than 2 megabars.

ALUMINUM

Aluminum is one of the exceptional metals which do not follow the linear shock relation of Equation 28. Instead, the shock relation for aluminum is expressed in a quadratic form as

$$U = a_1 + a_2 u + a_3 u^2 . \quad (34)$$

In addition, the adiabatic sound speed a is also a quadratic function of u :

$$a = b_1 + b_2 u + b_3 u^2 . \quad (35)$$

For simplicity, the coefficients a_i and b_i used in this study are obtained by fitting them into the table of Chou et al (Ref. 18) (see Table 1).

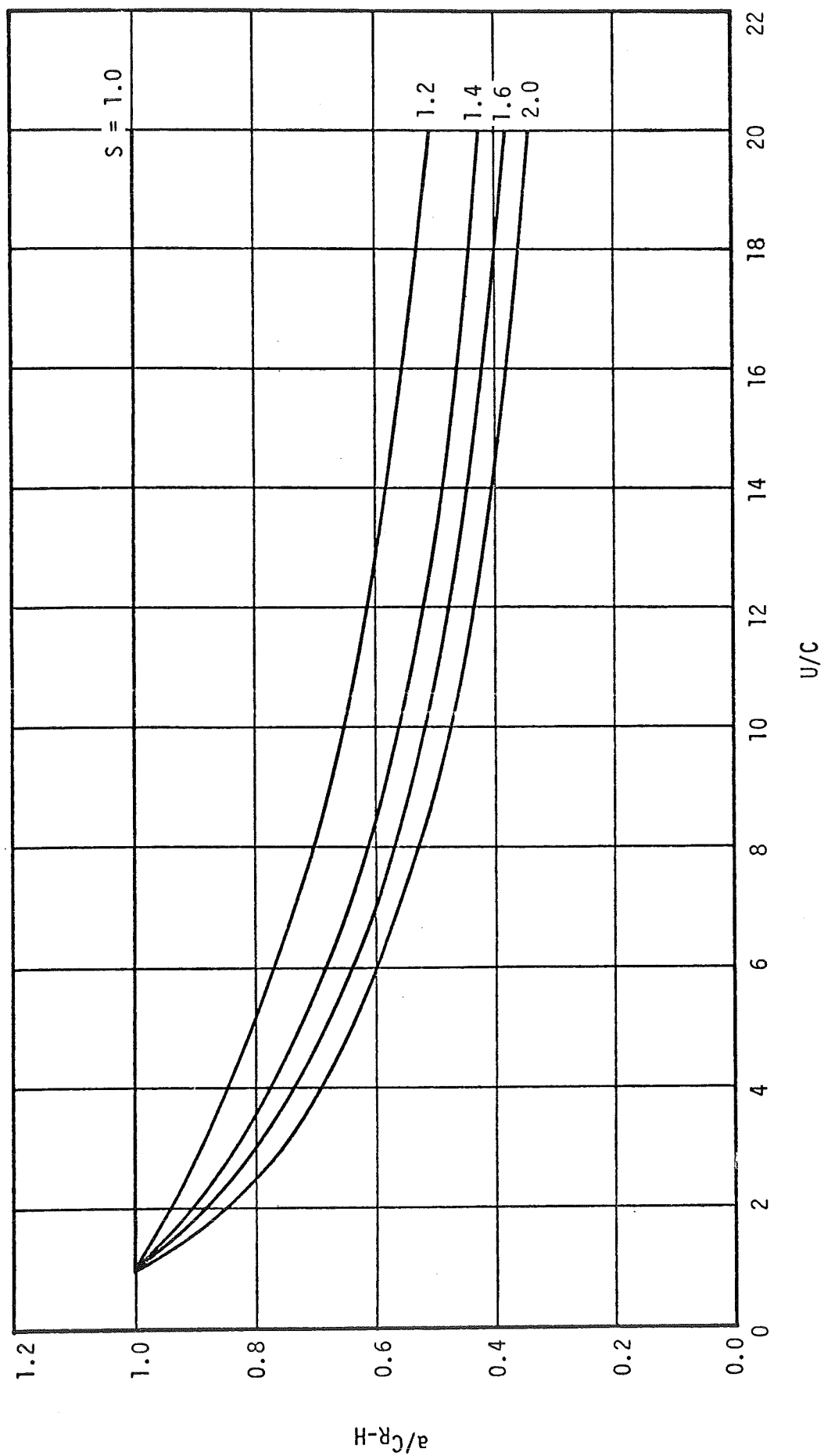


FIGURE 10. THE RATIO OF ADIABATIC SOUND SPEED AND THE SLOPE OF RANKINE-HUGONOT CURVE AS A FUNCTION OF SHOCK MACH NUMBER FOR c, s MATERIAL

TABLE 1. COEFFICIENTS OF EQUATIONS 34 AND 35

	<u>$u \leq 5.0$ (mm/μsec)</u>	<u>$u > 5.0$ (mm/μsec)</u>
a_1	5.985	5.278
a_2	1.237	1.503
a_3	-0.001	-0.0271
b_1	6.883	5.101
b_2	0.9849	1.518
b_3	-0.0084	-0.048

Chou's table was established by using the Tillotsen equation (Ref. 14) (for $p > 1$ mb) and the experimental data of the Los Alamos Laboratory (Ref. 16) (for $p \leq 1$ mb).

Again, Equation 34, combining Equations 24, 25, and 26, provides the shock relations needed in the next section.

SHOCK PROPAGATION LAWS

As mentioned previously, a shock velocity and area relation (Equation 1) or shock propagation law is needed for completing the characteristic solutions. Equation 1 is derived in this section.

A shock wave moving in a channel with varying cross-sectional area is considered. The shock strength attenuates if the channel area increases downstream; and conversely, the shock wave would be strengthened if the channel area converges. This phenomenon is well-known in blast wave theory. Even if the fluid is assumed frictionless, the shock front velocity decreases very quickly and approaches the velocity of sound at a large distance from the source of explosion. The enlargement of the shock front area results in attenuation of the shock strength, or, in the equivalent, a reduction of shock velocity. The shock propagation law relates the change of the shock velocity to the change of the channel area.

The shock propagation law was first obtained by Chester (Ref. 19) and Chisnell (Ref. 20) from a linearized approximation of one-dimensional compressible flows. Their results were later rederived by Whitham (Ref. 21) who applied a simple rule in the non-steady, one-dimensional flow theory. Their result is sometimes called "CCW Approximation". In this section a shock propagation law is formulated for solid media.

Whitman's rule can be stated as follows: the flow quantities along a characteristic line must be equal to the flow quantities just behind the shock wave. With this rule and the Hugoniot relation, a differential relation is obtained, which describes the motion of a shock wave down a nonuniform area channel. In hypervelocity impact problems, a plane shock is generated initially at the interface between

the projectile and the target, and the shock front area suddenly enlarges while it propagates into the target. Then the shock propagation law is applied under the assumption that the whole flow field is composed of a number of one-dimensional "rays" (see page 8), each one of which independently obeys this law.

For one-dimensional, unsteady flow in a variable area channel, the governing equations of the fluid flow may be written in the following form:

$$\frac{\partial \rho}{\partial t} + u \frac{\partial \rho}{\partial x} + \rho \left(\frac{\partial u}{\partial x} + \frac{u}{A} \cdot \frac{dA}{dx} \right) = 0 \quad , \quad (36)$$

$$\frac{\partial u}{\partial t} + u \frac{\partial u}{\partial x} + \frac{a^2}{\rho} \cdot \frac{\partial \rho}{\partial x} = 0 \quad , \quad (37)$$

and

$$\frac{\partial e}{\partial t} + u \frac{\partial e}{\partial x} - \frac{p}{\rho^2} \left(\frac{\partial \rho}{\partial t} + u \frac{\partial \rho}{\partial x} \right) = 0 \quad . \quad (38)$$

Applying the theory of characteristics to Equations 36 and 37 yields

$$\Gamma'_{\pm}, \quad d\rho \pm \frac{\rho}{a} du + \frac{\rho u}{A(u+a)} dA = 0 \quad (39)$$

on the characteristics

$$C'_{\pm}, \quad \frac{dx}{dt} = u \pm a$$

where Γ'_{\pm} denotes hodographic characteristics and C'_{\pm} denotes physical characteristics.

To apply Whitham's rule, the flow quantities on the outgoing characteristics C_+ are matched with the flow quantities behind the shock wave. The appropriate branch in Equation 39 is

$$\frac{d\rho}{\rho} + \frac{a}{u} \cdot \frac{d\rho}{\rho} + \frac{du}{u} + \frac{du}{a} + \frac{dA}{A} = 0 \quad . \quad (40)$$

The terms ρ , a , and u are functions of shock velocity U and the material characteristics. Equation 40 can thus be integrated and the integrated equation represents the shock propagation law.

For c, s material, Equation 40 becomes

$$\frac{dA}{A} = - \mu^2 (M_s) \frac{dU}{U} \quad (41)$$

where $M_s = U/c$ and

$$\begin{aligned} \frac{1}{\mu^2} &= \frac{1}{[1 + (s - 1) M_s]} + \frac{M_s}{M_s - 1} \\ &+ \frac{M_s}{\{[(s - 1) M_s + 1] [(3s - 1) M_s - (2s - 1)]\}^{\frac{1}{2}}} \\ &+ \frac{\{[(s - 1) M_s + 1] [(3s - 1) M_s - (2s - 1)]\}^{\frac{1}{2}}}{(M_s - 1) [1 + (s - 1) M_s]} \quad . \quad (42) \end{aligned}$$

For the case of strong shock, $M_s \equiv U/c \rightarrow \infty$, Equation 42 reduces to

$$\mu_\infty^2 = \frac{[(s - 1) (3s - 1)]^{\frac{1}{2}}}{1 + [(s - 1) (3s - 1)]^{\frac{1}{2}}} \quad . \quad (43)$$

For aluminum, the function μ^2 in Equation 41 is

$$\mu^2 = \frac{U(u+a)}{u} - \frac{1}{U} - \frac{1}{U-u} + \frac{1}{(U-u)(a_2 + 2a_3 u)} + \frac{1}{a(a_2 + 2a_3 u)} \quad (44)$$

where a and u are functions of U , as shown in Equations 34 and 35 of the previous section.

Integration of Equation 40 yields

$$A(U) = K \exp \left(- \int \mu^2 \frac{dU}{U} \right) \quad (45)$$

which is Equation 1 on page 8 . K is an integration constant.

Notice that the integration in Equation 45 can be carried out explicitly through a tedious procedure. But in actual computations, only the function μ is used. The computational procedures will be discussed in a later section.

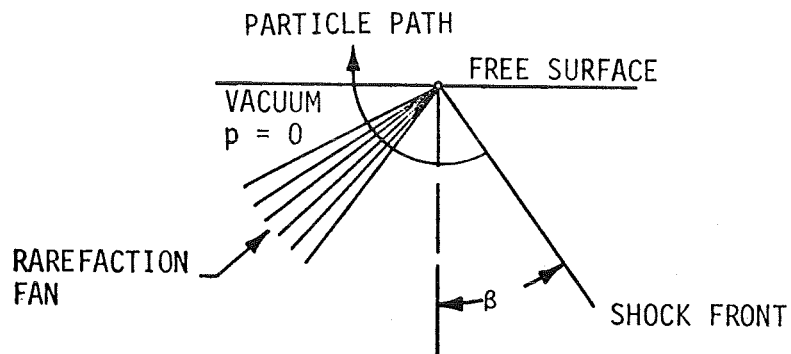
SHOCK WAVE INTERACTION WITH FREE BOUNDARY

As stated previously, information about shock-free surface interaction is required to specify one of the boundary conditions in constructing the characteristic solutions. Figure 11a shows an expansion fan behind the shock, through which the pressure drops from the value immediately behind the shock wave to zero at the tail of the fan. The physical picture is analogous to Prandtl-Meyer expansion around a convex corner except that the expansion fan is three-dimensional and unsteady in nature. The shock front would attenuate and is distorted by the rarefaction waves.

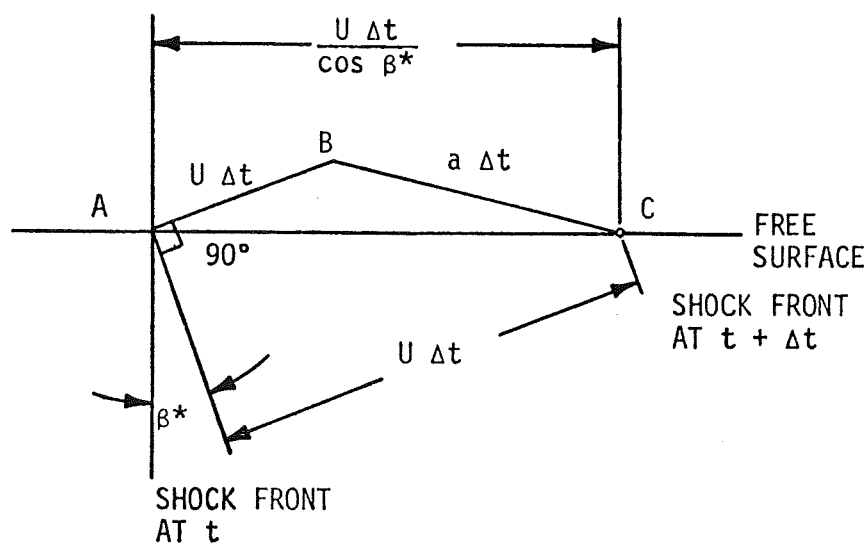
A simplified model has been proposed by Russian scientists (Ref. 22) to estimate the shock inclination. Recently, Rae (Ref. 7) applied it to the impact-generated shock propagation, but he chose ideal gases in the formulation. In the present study, Rae's formulation is generalized to solid media.

From Figure 11b, if the shock inclination β is greater than a certain value β^* , called the "critical angle", the rarefaction waves cannot reach the shock front. Therefore, if the original shock inclination $\beta > \beta^*$, the shock motion along the free surface will not be affected by the free surface interaction. Conversely, if $\beta < \beta^*$, β will change continuously and eventually approaches β^* . The shock will remain undistorted afterward.

The transition phenomenon ($\beta \rightarrow \beta^*$) is rather complex in mathematical analysis, because an unsteady and three-dimensional flow problem is involved. In this work, it is assumed that the transition period is so short in the development of shock profiles that it can be neglected. Then $\beta = \beta^*$ will provide the boundary condition at the free surface; β^* depends on the local shock strength and is derived by Equation 46.



(a) EXPANSION BEHIND THE SHOCK FRONT



(b) CRITICAL ANGLE β^*

FIGURE 11. SHOCK WAVE AND FREE SURFACE INTERACTION

Referring to Figure 11b, the cosine law gives

$$\overline{BC}^2 = \overline{AB}^2 + \overline{AC}^2 - 2 \overline{AB} \cdot \overline{BC} \cos \beta^*$$

or

$$a^2 = u^2 + U^2 / \cos^2 \beta^* - 2 u U$$

and

$$\beta^* = \cos^{-1} \left[\left(\frac{a^2}{U^2} - \frac{2u}{U} + \frac{u^2}{U^2} \right)^{-\frac{1}{2}} \right] \quad . \quad (46)$$

Equation 46 indicates the critical shock inclination angle β^* , as a function of U , u , and a . Since a and u can be expressed in terms of U ; β^* actually depends on shock velocity U only.

CONSTRUCTION OF NUMERICAL SOLUTIONS FOR SHOCK WAVE PROPAGATIONS

INITIAL NORMAL SHOCK WAVES

When a projectile impacts on a target with relative velocity V , two normal shock waves are generated at the interface and move in opposite directions with respect to the interface (Figure 12a). The normal shock solutions can be obtained by applying Equations 24, 26, and 28 or 34.

For similar material hypervelocity impacts, the particle velocity equals to half of the impact velocity (Figure 12b),

$$u_3 = u_2 = V/2 \quad . \quad (47)$$

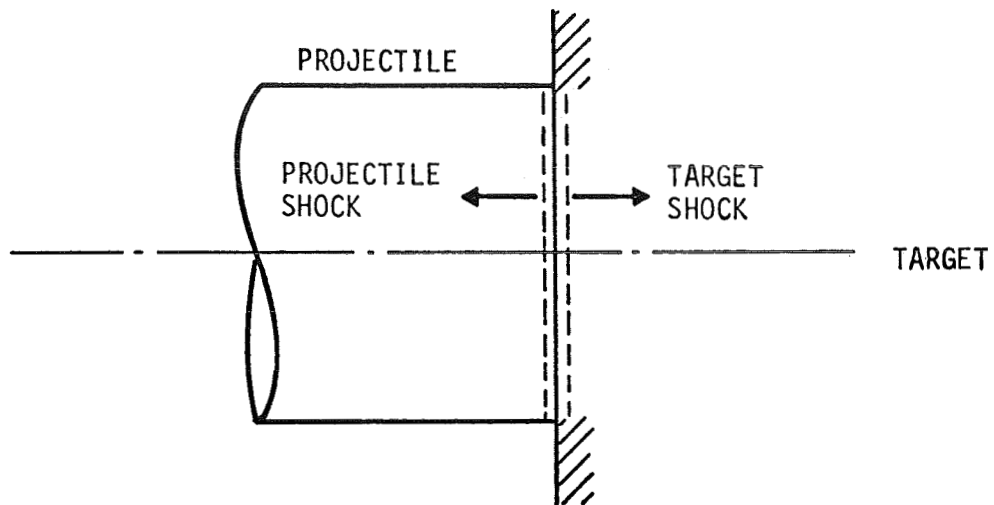
Equation 47 is derived by taking a velocity transformation. If the projectile and the target move in opposite directions with the same speed $V/2$, the fluid particles behind the shock waves should be motionless as a result of symmetry with respect to the transformed coordinate system.

For nonsimilar material impacts, a contact discontinuity interface exists. But the pressure and velocity functions are assumed continuous across the interface; $p_3 = p_2$ and $u_3 = u_2$. From Equation 25,

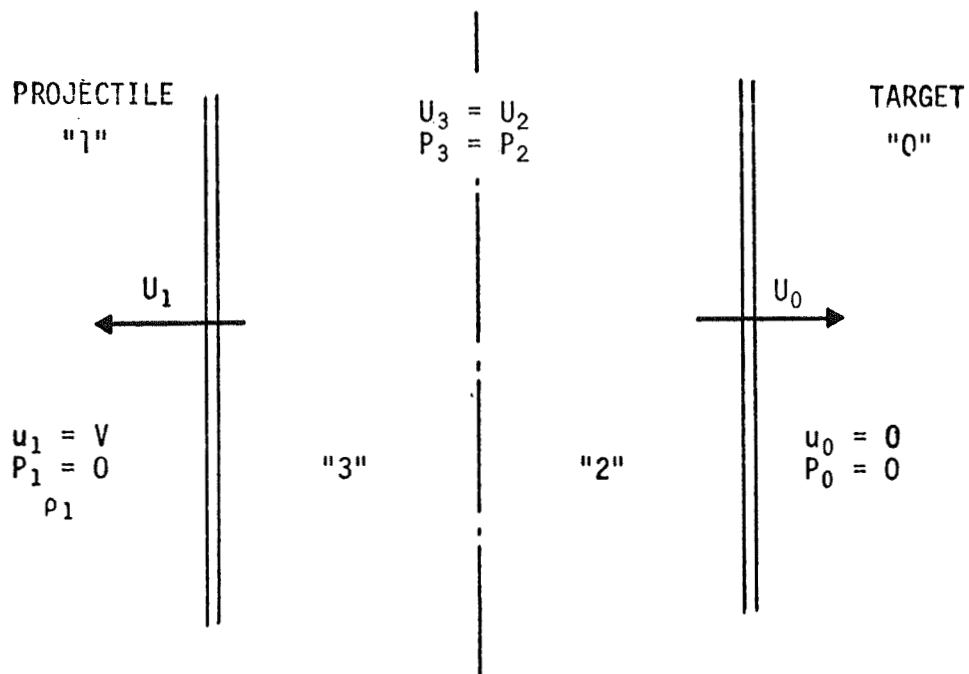
$$p_2 = \rho_0 u_2 U_0 \quad (48)$$

and

$$p_3 = \rho_1 (V - u_3) (V - U_1) \quad .$$



(a) NORMAL SHOCKS GENERATED IMMEDIATELY AFTER IMPACT



(b) NORMAL SHOCK MECHANISM

FIGURE 12. IMPACT-GENERATED NORMAL SHOCK WAVES

With the aid of shock relations, Equation 28 or 34, the solutions of U_1 and U_0 are readily found.

SIMPLE WAVE SOLUTIONS

As shown in Figure 13, U_0 is assumed to be the normal shock velocity calculated in Equation 47 or Equation 48. Then the "Mach angle" m_0 can be obtained from Equations 15 and 41,

$$m_0 = \tan^{-1} [\mu(U_0)] , \quad (49)$$

and

$$\theta_0 = 0 .$$

Next, a shock velocity U_1 is chosen such that $U_1 < U_0$, and m_0 is calculated from Equation 49. The shock angle θ_1 is

$$\theta_1 = \int_{U_0}^{U_1} \frac{dU}{U \mu(U)} . \quad (50)$$

The shock position of point 1 is determined by

$$\frac{x_1}{t} = U_1 \cos(\theta_1 + m_1) / \cos m_1$$

and

$$\frac{y_1}{t} = U_1 \sin(\theta_1 + m_1) / \cos m_1 \quad (51)$$

where t is the time after impact.

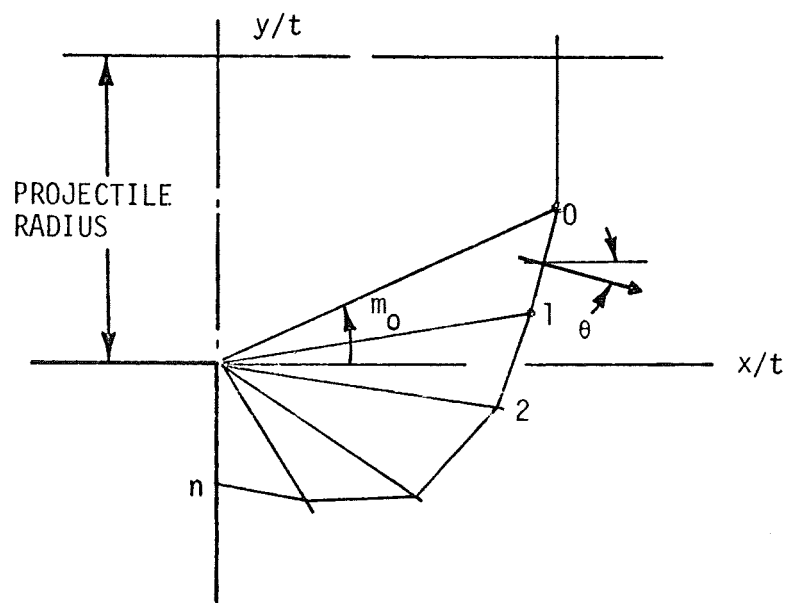


FIGURE 13. CONSTRUCTION OF A SIMPLE WAVE SOLUTION

Repeating the procedure, by choosing a sequence of shock velocities U_2, U_3, \dots, U_n , $m_i, \theta_i, x_i/t, y_i/t$ ($i = 2, \dots, n$) are determined in the same manner. The computations continue until $x_0/t = 0$. This completes the construction of a simple wave solution.

ASYMPTOTIC SOLUTION OF TWO-DIMENSIONAL SHOCK PROFILES FOR STRONG SHOCK

An analytic expression of shock profiles can be obtained for large U in simple wave solutions. c, s material is chosen in the formulation that follows.

The function $\mu(U)$ for a c, s material in the shock propagation law approaches a constant as $U \rightarrow \infty$ (Equation 43), and is denoted by μ_∞ . Therefore

$$\theta = \frac{1}{\mu_\infty} \int_U^{U_0} \frac{dU}{U} = \frac{1}{\mu_\infty} \ln (U/U_0)$$

and

$$U = U_0 e^{\mu_\infty \theta} \quad . \quad (52)$$

The shock wave locus is in the form

$$\frac{x}{U_0 t} = e^{\mu_\infty \theta} \cos (\theta + m_\infty) / \cos m_\infty$$

and

$$\frac{y}{U_0 t} = e^{\mu_\infty \theta} \sin (\theta + m_\infty) / \cos m_\infty \quad (53)$$

where $m_\infty = \tan^{-1} \mu_\infty$ is a constant.

Letting $R = (x^2 + y^2)^{\frac{1}{2}}$, Equation 53 may be expressed in polar coordinates as

$$R = k e^{\mu_{\infty} \varphi} \quad (54)$$

where

$$\varphi = \theta + m_{\infty}$$

$$k = \frac{U_0 t}{\cos m_{\infty}} e^{-m_{\infty}}.$$

Equation 54 (see Figure 14) represents a logarithmic spiral curve, and has been derived by Skew (Ref. 10) for an ideal gas. However; it should be emphasized that Equation 52 must be used with caution since the simple linear shock relation of c, s material may not be valid for very strong shocks.

FINITE DIFFERENCE SOLUTIONS FOR THE CHARACTERISTIC EQUATIONS

For an axisymmetric impact problem, the simple wave solution only provides the initial condition. Two boundary conditions are used:

- $\theta = 0$ at the axis of symmetry
- $\theta = - \left(\beta^* + \frac{\pi}{2} \right)$ on the free surface.

The method of characteristics is applied in computing the shock profiles. To do this, the characteristic equations, Equations 22 and 23, are first written in finite difference forms, and the solutions are then constructed by using the numerical techniques of compressible flow theory (Ref. 14).

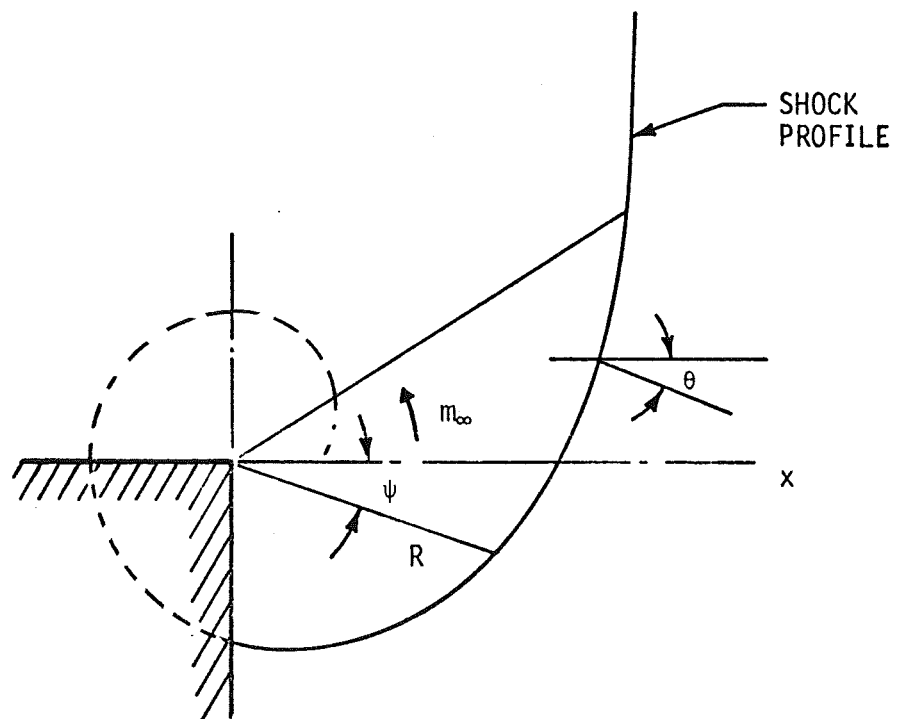


FIGURE 14. APPROXIMATE SHOCK PROFILE FOR THE STRONG SHOCK SITUATION (U LARGE)

The finite difference scheme developed herein differs from the conventional method. The present scheme is designed to construct the shock profiles for successive time intervals. Instead of using two known field points to obtain the third new point, only one point and the time interval Δt are chosen to determine a new point. The advantage in this numerical scheme is that the successive shock profiles as a function of time can be directly computed without interpolations between the field points. The resultant finite difference equations are programmed on the IBM 1130 digital computer and results will be presented in a later section.

AN APPROXIMATION FOR PRESSURE PULSE AT LATE STAGE OF IMPACT

The shortcoming on the present shock propagation model is that no information is given the flow variables behind the shock wave. The flow field of a diffracting shock wave is too complicated to be obtained analytically. Probably this is the reason for the development of direct numerical programs, such as PIC code and Eulerean Code, since the flow variables are significant in the description of the impact mechanism.

At the late stage of shock propagation, it is found that the shock front develops rapidly into a sphere-like shape, and the flow variables vary gradually around the shock front. These facts suggest that it is possible to obtain an approximation for the flow field at the large elapsed time.

To find the approximate solutions in the flow field, the equations for three-dimensional, unsteady flow with symmetric axis are written in a spherical coordinate system. These equations are

$$\frac{\partial u_r}{\partial t} + u_r \frac{\partial u_r}{\partial r} + \frac{u_\varphi}{r} \cdot \frac{\partial u_r}{\partial \varphi} - \frac{v^2}{r} + \frac{1}{\rho} \frac{\partial p}{\partial r} = 0$$

$$\frac{\partial u_\varphi}{\partial t} + u_r \frac{\partial u_\varphi}{\partial \varphi} + \frac{u_\varphi}{r} \cdot \frac{\partial u_\varphi}{\partial \psi} + \frac{u_\varphi u_r}{r} + \frac{1}{\rho r} \cdot \frac{\partial p}{\partial \varphi} = 0 \quad (55)$$

$$\frac{\partial \rho}{\partial t} + u_r \frac{\partial \rho}{\partial r} + \frac{u}{r} \cdot \frac{\partial \rho}{\partial \varphi} + \rho \frac{\partial u_r}{\partial r} + \frac{1}{r} \frac{\partial u_r}{\partial \varphi} + \frac{\partial u_r}{r} + \frac{u_\varphi}{r} \cos \varphi = 0$$

$$\frac{\partial e}{\partial t} + u_r \cdot \frac{\partial e}{\partial r} + \frac{u_\varphi}{r} \cdot \frac{\partial e}{\partial \varphi} - \frac{p}{\rho^2} \frac{\partial \rho}{\partial t} + u_r \frac{\partial \rho}{\partial t} + \frac{u_\varphi}{r} \cdot \frac{\partial e}{\partial \varphi} = 0$$

where u_r and u_φ represent the velocity components in the r and φ directions, respectively (Figure 15).

Expanding the variable u_r , u_θ , ρ , and p in Fourier series yields

$$u_r(r, \varphi, t) = u_0(r, t) + \sum_{n=1}^{\infty} u_n(r, t) \cos n\theta \quad (56)$$

$$u_\theta(r, \varphi, t) = \sum_{n=1}^{\infty} v_n(r, t) \sin n\theta, \text{ etc.}$$

By substituting Equation 56 in Equation 55, the zeroth order equations are obtained:

$$\frac{\partial \rho}{\partial t} + \rho \frac{\partial u}{\partial r} + u \frac{\partial \rho}{\partial t} + \frac{\partial \rho u}{r} = 0$$

$$\frac{\partial u}{\partial t} + u \frac{\partial u}{\partial r} + \frac{1}{\rho} \cdot \frac{\partial p}{\partial r} = 0 \quad (57)$$

$$\frac{\partial e}{\partial t} + u \frac{\partial \rho}{\partial t} - \frac{p}{\rho} \frac{\partial \rho}{\partial t} + u \frac{\partial \rho}{\partial r} = 0 \quad .$$

In the above system of equations, $u = u_r$ and the subscript "o" is dropped.

Equation 57 is identified as a one-dimensional, unsteady flow equation system. A transformation of the dependent and independent variables is introduced as

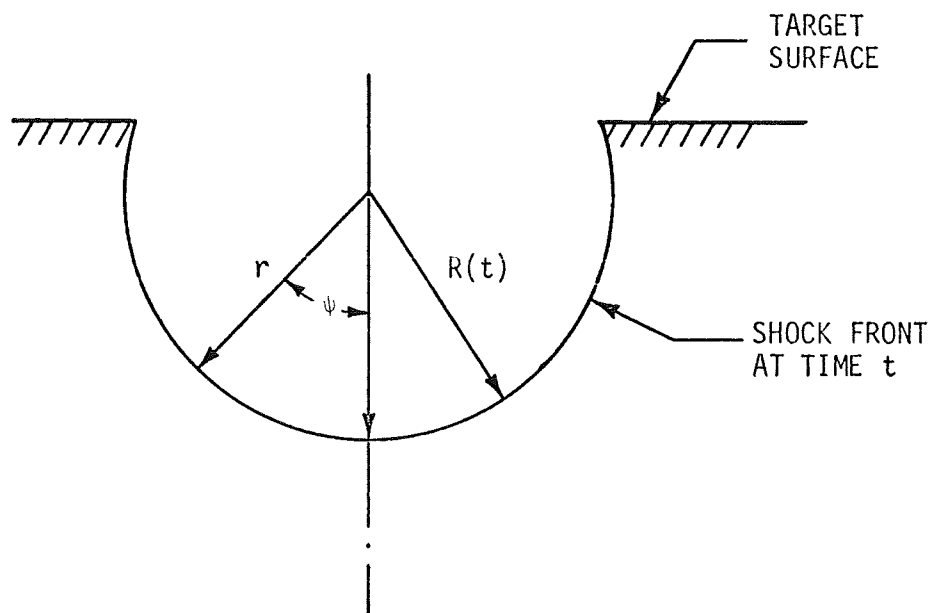


FIGURE 15. SPHERICAL COORDINATE SYSTEM WITH SYMMETRIC AXIS

$$u = U f ,$$

$$p = \rho_0 U^2 g ,$$

$$\rho = \rho_0 h ,$$

$$\xi = \frac{r}{R} , \tag{58}$$

$$\lambda = \frac{R}{U} \cdot \frac{dU}{dR}$$

and

$$U = \frac{dR}{dt} ,$$

where R is the shock front position. The first two equations of Equation 57 become

$$(f - \xi) \frac{\partial h}{\partial \xi} + h \frac{\partial f}{\partial \xi} + \frac{2fh}{\xi} = -\lambda U \frac{\partial h}{\partial U} \tag{59}$$

$$(f - \xi) \frac{\partial f}{\partial \xi} + \lambda f + \frac{1}{h} \frac{\partial g}{\partial \xi} = -\lambda U \frac{\partial f}{\partial U} . \tag{60}$$

Note that f , g , and h are functions of two variables; ξ and $R(t)$. Solution of the above system of equations is still a very difficult task. In general, the similarity solutions do not exist because the assumption of strong condition may not be justified. In fact, when the impact-generated shock wave becomes a spherical shape, the shock strength is usually weak.

Now, two assumptions are imposed:

$$f = f_1 \xi$$

$$\frac{\partial h}{\partial U} = \frac{h}{h_1} \cdot \frac{dh_1}{dU}$$

where f_1 , h_1 are the functions evaluated at the shock front ($\xi = 1$) and they are time-dependent functions.

The first assumption is made because the numerical solutions of other studies (Refs. 8 and 23) show that the velocity functions are nearly linear*, while the second assumption is based on a quasi-similarity theory by Oshima (see Ref. 12).

From Equations 59 and 60, combined with the assumptions above, g and h are readily obtained:

$$\begin{aligned} g &= \tilde{A} \left(\xi^{\tilde{m}+2} - 1 \right) + g_1 \\ h &= h_1 \xi^{\tilde{m}} \end{aligned} \tag{61}$$

where $g_1 = g(1, t)$ and \tilde{A} , \tilde{m} are functions of f_1 , g_1 , h_1 , and λ .

In terms of physical quantities, the solutions are

$$\begin{aligned} u &= u_1 r/R \\ \rho &= \rho_1 (r/R)^{\tilde{m}} \\ p &= \rho_0 U^2 \tilde{A} \left[\left(\frac{r}{R} \right)^{\tilde{m}+2} - 1 \right] \end{aligned} \tag{62}$$

*The first assumption was also made by Rayzer (Ref. 24) and Sakura (Ref. 12).

where

$$\tilde{m} = \frac{3 u_1 / U + \lambda U / \rho_1 \cdot \frac{\rho}{\partial U}}{(u_1 - U) / U}$$

and

$$\tilde{A} = \frac{\rho_1}{\rho_0} \left[\frac{u_1}{U^2} (u_1 - U) + \frac{\lambda u_1}{U} + U \frac{\partial (u_1 / U)}{\partial U} \right] / (\tilde{m} + 2) .$$

The subscript ₁ denotes the Hugoniot flow quantities.

NUMERICAL RESULTS AND DISCUSSION

In this section, some numerical results are presented. Based on these results, discussions are given on the theoretical model proposed in this study. Since some of the assumptions imposed in this model are subjected to question, it is necessary to compare the present results carefully with numerical data available from other studies. Because of the complexity inherent in this problem, the justification of some assumptions can be achieved only through such a comparison.

THE STARTING POINT OF SHOCK CURVATURE

In Whitham's rule, the effect of disturbances behind the shock wave is ignored. The justification of this model is difficult to establish because the information on the flow field behind the shock wave is still meager.

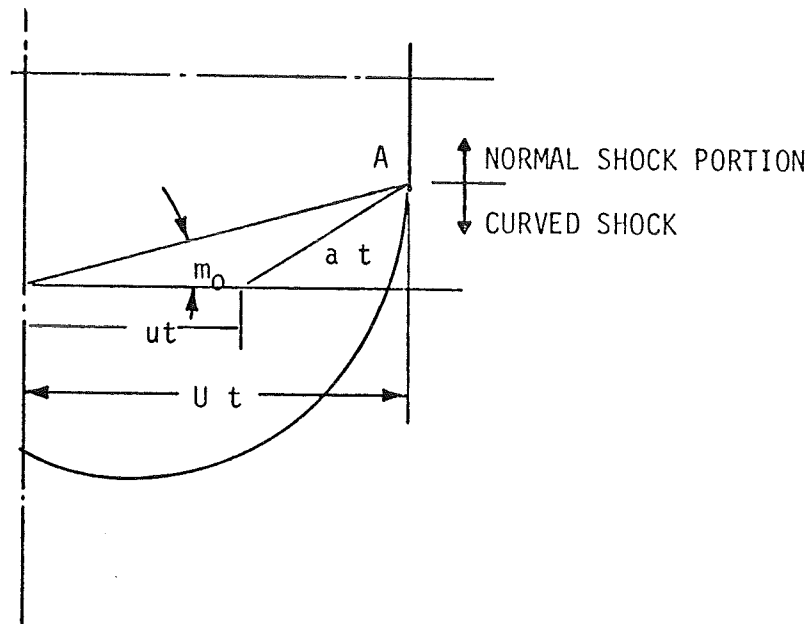
Point A in Figure 16a represents the location where the shock curvature starts. By the CCW approximation, the following is obtained:

$$\tan m_0 = \mu(U_0) \quad .$$

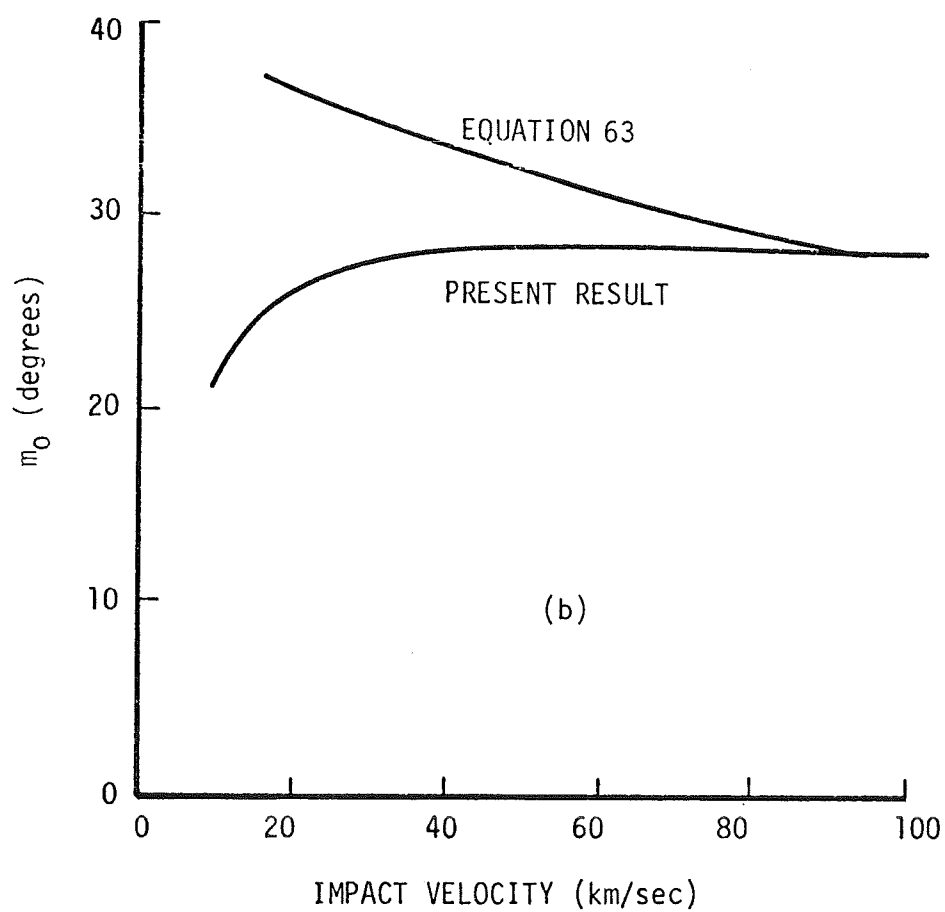
But m_0 can also be predicted by an alternative equation:

$$\tan m_0 = \frac{a}{U} \left[1 - \left(\frac{U - u}{a} \right)^2 \right]^{\frac{1}{2}} \quad . \quad (63)$$

Equation 63 was derived by Skew (Ref. 25) and also by Heyda (Ref. 26) to indicate the point at which the normal shock wave is first reached by the rarefaction wave from a turning corner. It must be pointed out that Equation 63 is only an approximation because the



(a)



(b)

FIGURE 16. THE STARTING POINT OF SHOCK CURVATURE IN ALUMINUM

velocity u and sound velocity a depend on the locations behind the shock wave.

A comparison of the above two approximations is shown in Figure 16b. For high impact velocities, the discrepancy between these two predictions is small, but large discrepancy exists in the low velocity region. Skew (Ref. 23) performed an experiment for shock waves diffracting around a corner. Observation of the shock shape favors the prediction of Equation 63. This may imply that this is not a definite conclusion since the impact-generated shock waves in solids may be different from the compressible flow waves in Skew's experiment.

THE SUCCESSIVE POSITIONS OF SHOCK PROFILES

A numerical example of aluminum impact on aluminum at a velocity of 20 km/sec is presented in Figure 17 that the positions of shock profiles are functions of successive time steps. The normal shock portion vanishes very rapidly and it completely disappears at about 5.5 microseconds. The shock profile develops further into an ellipsoid and eventually approaches a hemispherical shape.

The appearance of hemispherical shock shape inspires the assumption of spherical symmetry made by many investigators (see (Ref. 7)). This assumption is justified only if, after a long period of time, the shock strength has attenuated considerably and degenerated into the speed of sound. Soon after impact, the shock shape is far from spherical and the flow properties vary along the shock front. The pressure distribution, for instance, has the highest value at the symmetric axis and decreases in value toward the target free surface.

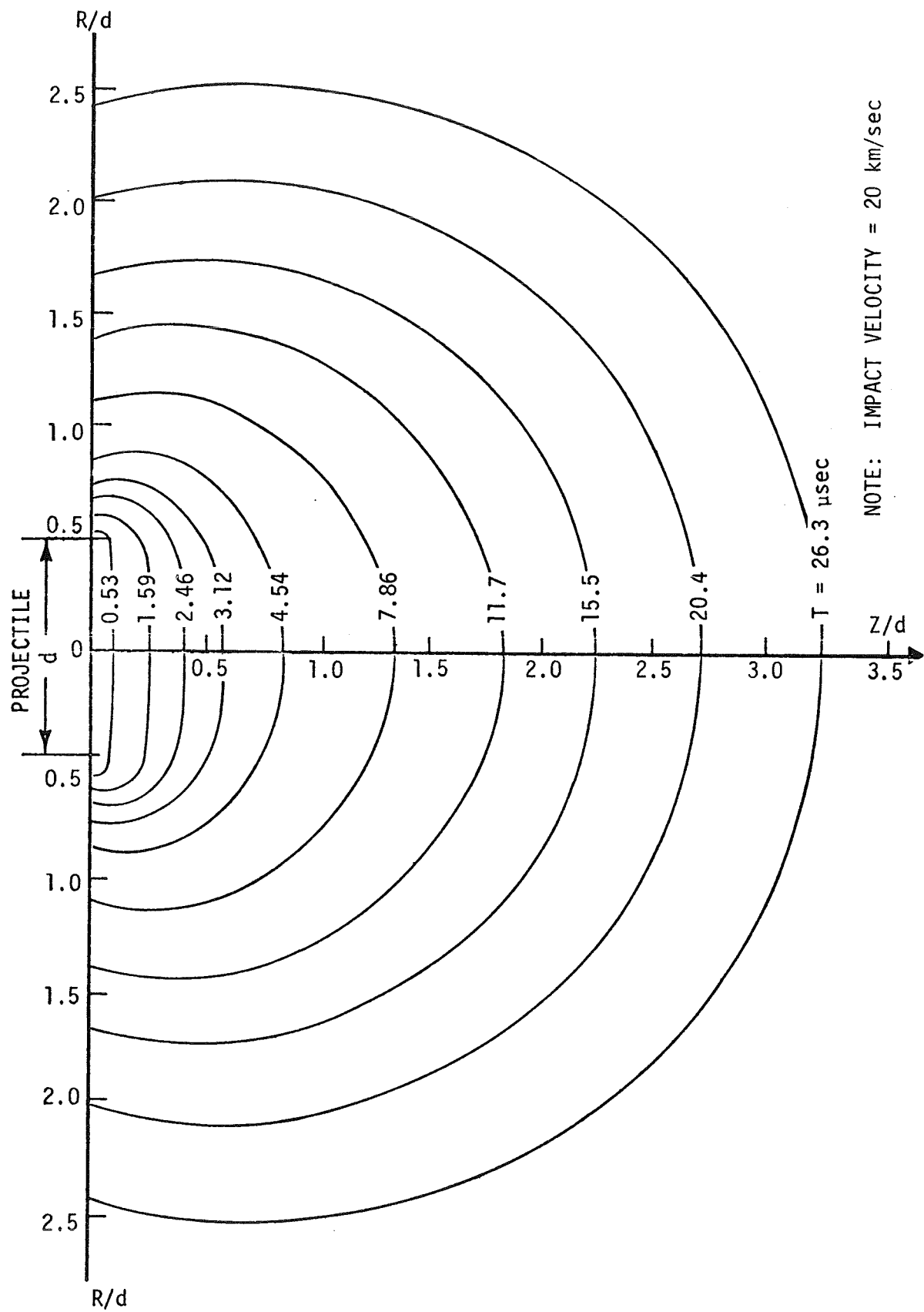


FIGURE 17. SUCCESSIVE SHOCK PROFILES FOR ALUMINUM-ON-ALUMINUM IMPACT

PRESSURE DISTRIBUTIONS

A comparison is made with the numerical results obtained by Heyda and Riney (Ref. 27) concerning the peak pressure along the axis of cylindrical symmetry. Figure 18 shows that for $(z/d) < 1$ the pressure is equal to Hugoniot pressure obtained by the normal shock relation since the plane shock generated at the interface has not been affected by the rarefaction waves from the corner. The pressure then decreases drastically as the shock wave advances into the target. The discrepancy of these two results at the early stage is mainly caused by the "numerical diffusion" effect inherent in the direct numerical scheme. Errors of about 30 percent occur compared with the exact solutions. However, the agreement in general is good except the late stage in which the present solution is consistently higher than the direct numerical solutions. This is believed to occur when the rarefaction waves reflected from the rear surface of the projectile are not considered. Such rarefaction waves are known to attenuate the target shock strength (Ref. 18).

The angular distributions of shock pressure are shown in Figure 19 so that the pressure gradients in ψ -direction are indeed small for large elapsed time. This phenomenon provides the basis of formulating the quasi-similarity solutions in the previous section.

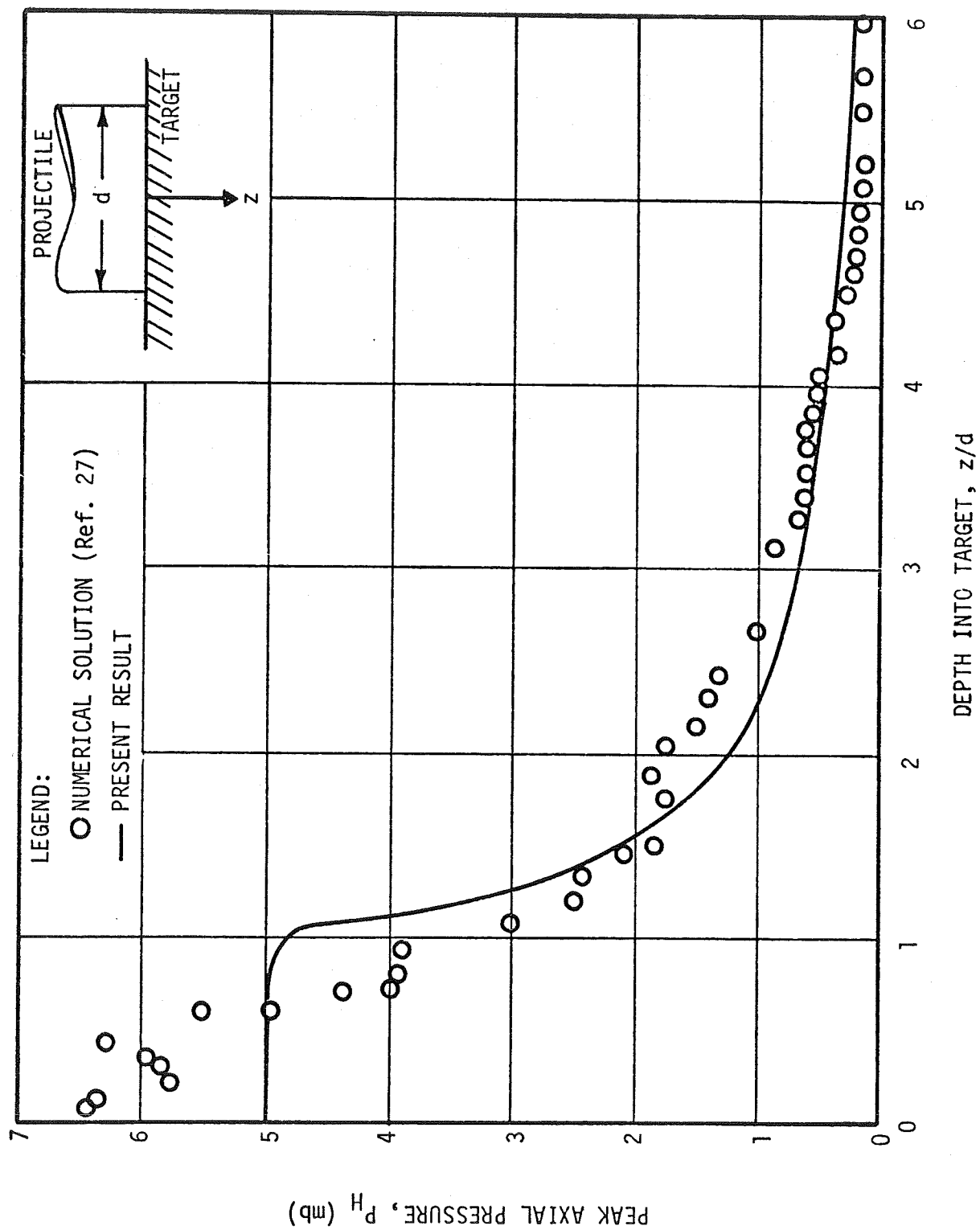


FIGURE 18. COMPARISON OF PEAK PRESSURE DISTRIBUTION FOR ALUMINUM-ON-ALUMINUM IMPACT

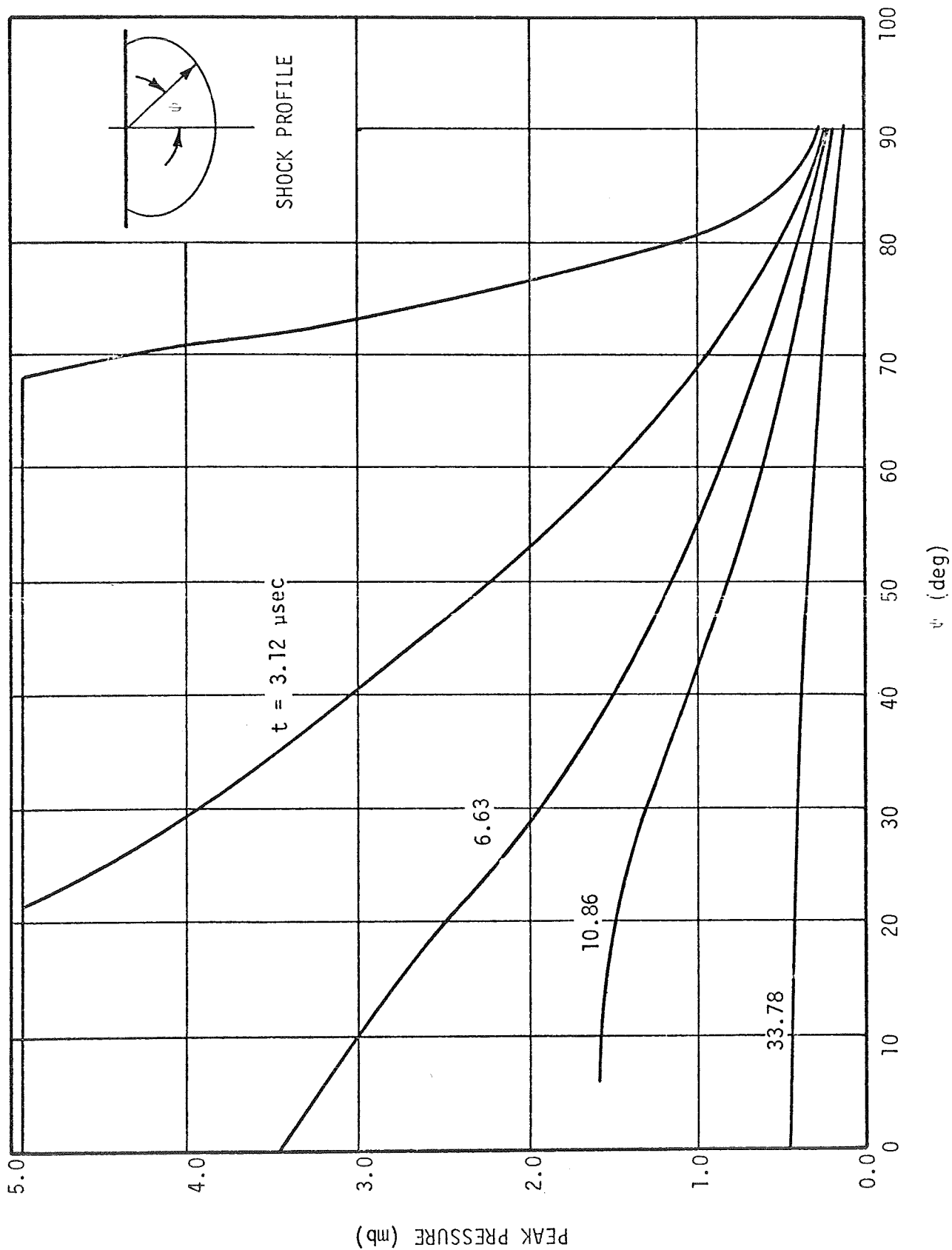


FIGURE 19. ANGULAR PRESSURE DISTRIBUTION

SUMMARY

A theoretical model based on shock diffraction and blast wave theories is developed to describe the propagation of impact-generated shock waves in solid materials. The successive positions of two-dimensional and axisymmetric shock profiles are obtained by using the method of characteristics. The present analytical model, which differs from the usual numerical approaches, such as PIC and OIL codes, can eliminate the unrealistic cell pressure fluctuations caused by numerical diffusion.

Limited comparisons with the existing numerical results are satisfactory although not conclusive. More comparisons, especially low impact velocity ranges, are necessary to reach a definite conclusion.

The rarefaction wave reflected from the back surface of the projectile is ignored in the present study. It is anticipated that such rarefaction wave can alter the strength and the shape of the target shock. Moreover, the flow variables in the shock region are also affected by such rarefaction waves. Further investigations on the rarefaction effects in the target are recommended.

APPENDIX. SOUND SPEED OF c, s MATERIAL BEHIND THE SHOCK

The Mie-Grüneisen equation of state is

$$p - p_0 = \rho \Gamma(\rho) (e - e_0) \quad (\text{A-1})$$

where the subscript 0 denotes the initial state and $\Gamma(\rho)$, the Grüneisen ratio, is a function only of density. Differentiating Equation A-1 with respect to e at constant ρ , the following expression for $\Gamma(\rho)$ in terms of thermodynamic quantities is obtained:

$$\Gamma = \frac{1}{\rho} \left(\frac{\partial p}{\partial e} \right)_\rho \equiv \frac{1}{\rho C_V} \left(\frac{\partial p}{\partial T} \right)_\rho \quad (\text{A-2})$$

According to Reference 7, $\Gamma \approx 2s - 1$ at normal density, or pressure $p = 0$. But for higher pressure, a constant value of Γ was proposed by Rae (Ref. 7), who matched the Mie-Grüneisen equation of state with the Rankine-Hugoniot Relation of c, s material at very high shock strength. It is

$$\Gamma = 2(s - 1) \quad (\text{A-3})$$

It should be pointed out here that the range of validity of this expression of Γ is uncertain since there is no way to justify it by means of the available experimental data of metals. In spite of this, Equation A-3 is used in this work for the sake of convenience.

Now, a thermodynamic relation can be derived to yield the adiabatic sound speed as a function of dilatational wave speed c and the material parameter s . The derivation presented here is based on Reference 28. To do this, the Rankine-Hugoniot equation is differentiated first as follows.

$$de = \frac{1}{2} \left[\left(\frac{1}{\rho_0} - \frac{1}{\rho} \right) dp - (p + p_0) d\left(\frac{1}{\rho}\right) \right] . \quad (A-4)$$

Combined with the second law of thermodynamics, Equation A-4 becomes

$$T dS = de + p d\left(\frac{1}{\rho}\right) = \frac{1}{2} \left[\left(\frac{1}{\rho_0} - \frac{1}{\rho} \right) dp - (p - p_0) d\left(\frac{1}{\rho}\right) \right] . \quad (A-5)$$

A general expression of the equation of state may be written

$$p = p(\rho, S) ;$$

hence

$$dp = \left(\frac{\partial p}{\partial \rho} \right)_S d\rho + \left(\frac{\partial p}{\partial S} \right)_\rho dS , \quad (A-6)$$

where $\left(\frac{\partial p}{\partial \rho} \right)_S = a$ is the adiabatic sound speed, and

$$\left(\frac{\partial p}{\partial S} \right)_\rho \equiv \left(\frac{\partial p}{\partial T} \right)_\rho \left(\frac{\partial T}{\partial S} \right)_\rho = \frac{T}{C_v} \left(\frac{\partial p}{\partial T} \right)_\rho . \quad (A-7)$$

Substituting Equation A-3 into Equation A-7 yields

$$\left(\frac{\partial p}{\partial S} \right)_\rho = \rho T \Gamma . \quad (A-8)$$

Then Equation A-6 can be written as

$$dp = a^2 d\rho + \rho \Gamma T dS . \quad (A-9)$$

Eliminating the term $T dS$ from Equations A-5 and A-9 gives a relation between the adiabatic sound speed, a^2 , and the slope of the Rankine-Hugoniot curve in (p, ρ) plane, c^2_{R-H} , which is

$$c^2_{R-H} \equiv \frac{dp}{d\rho} = \frac{a^2 - (p - p_0)/2\rho}{1 - \rho \left(\frac{1}{\rho_0} \right) - \left(\frac{1}{\rho} \right) / 2}$$

or

$$a^2 = c^2_{R-H} \left[1 - \frac{\Gamma}{2} \left(\frac{\rho}{\rho_0} - 1 \right) \right] + \frac{\Gamma}{2} \left(\frac{p}{\rho_0 c^2} \right) \left(\frac{\rho_0}{\rho} \right) c^2 \quad . \quad (A-10)$$

The shock relations of c , s materials can be expressed as follows

$$U = c + sU$$

$$\frac{\rho_1}{\rho_0} = \frac{s M_s}{1 + (s - 1) M_s} \quad (A-11)$$

$$\frac{p_1}{\rho_0 c^2} = \frac{M_s (M_s - 1)}{p}$$

and

$$\begin{aligned} c^2_{R-H} &\equiv \frac{dp}{d\rho} \equiv \frac{dP/c/M_s}{d\rho/c/M_s} \\ &= \frac{c^2}{s^2} (2M_s - 1) [1 + (s - 1)M_s]^2 \end{aligned}$$

where $M_s = U/c$.

Substituting Equation A-11 in Equation A-10 yields

$$a = \frac{c}{s} [(3s - 1)(s - 1) M_s^2 - (2s^2 - 6s + 2)M_s - (2s - 1)]^{\frac{1}{2}} \quad (\text{A-12})$$

and

$$\frac{a}{c_{R-H}} = \left[\frac{(3s - 1) M_s - (2s - 1)}{(2M_s - 1) \cdot 1 + (s - 1) M_s} \right]^{\frac{1}{2}} \quad (\text{A-13})$$

The ratio of a/c_{R-H} depends upon s and M_s only.

REFERENCES

1. Bjok, R. L., "Effect of a Meteoroid Impact on Steel and Aluminum in Space", The Rand Corporation, P-1662, December 1958
2. Walsh, J. M. and J. H. Tillotson, "Hydrodynamic of Hypervelocity Impact", General Dynamics, General Atomic Division GA-3827, 1961
3. Riney, T. D., "Depth of Penetration of Hypervelocity Projectiles", AIAA Journal, 3, pp. 52-60, 1965
4. Johnson, W. E., "OIL-A Continuous Two-Dimensional Eulerian Hydrodynamic Code", General Dynamics Corporation, General Atomic Division, GAMD-5580, Revised January 1965
5. Young, C. T. K. and H. L. Cronkhite, "A Particle-in-Cell Program for the Calculation of the Phenomena of Hypervelocity Impacts", Brown Engineering Company, Inc., Technical Note AST-282, 1968
6. Kreyenhagan, K. N., M. H. Wagner, and R. L. Bjok, "Ballistic Limit Determination in Impacts on Multi-Material Laminated Targets", AIAA Journal Paper No. 69-356, 1968
7. Rae, N. J., "Analytic Studies of Impact-Generated Shock Propagation - Survey and New Results", Cornell Aeronautical Laboratory Report No. AL-2456-A-1, June 1968
8. Bach, G. G. and J. H. Lee, "Shock Propagation in Solid Media", AIAA Paper No. 67-141, 1967
9. Zeldovich, Y. B., "Motion of a Gas Due to a Pressure of Short Duration (Shock)", Akustichsky Zhurnal, 2, 1956, Translation in Soviet Physics-Acoustics, 2 (1956)
10. Skews, B. W., "Profiles of Diffracting Shock Waves: An Analysis Based on Whitham's Theory", University of Wetwatersrand, 1966
11. Hayes, W. D., "The Propagation Upward of the Shock Wave from A Strong Explosion in the Atmosphere", Journal of Fluid Mechanics, 32, Part 2, p. 317-331, 1968

12. Sakura, A., "The Blast Wave Theory", Basic Development in Fluid Mechanics, ed. by H. Holt, Academic Press, New York, New York, 1965
13. Whitham, G. B., "A New Approach to Problems of Shock Dynamics, Part I - Two-Dimensional Problems", Journal of Fluid Mechanics, 2, p. 145-171, 1957
14. Shapiro, A. H., The Dynamics of Thermodynamics of Compressible Fluid Flow, Volumes I and II, Ronald Press Company, New York, 1953
15. Tillotsen, J. H., "Metallic Equations of State for Hypervelocity Impact", General Atomic, GA-3216, July 1962
16. McQueen, R. G. and S. P. March, "Equation of State for Nineteen Metallic Elements From Shock-Wave Measurements to Two Megabars", Journal of Applied Physics, 31, 7, July 1960
17. Rice, M. H., R. G. McQueen, and J. M. Walsh, Compression of Solid by Strong Shock Waves, Sietz and Turnbull Series, Volume 6, Solid State Physics, Academic Press, 1958
18. Chou, P. C. and F. E. Allison, "Strong Plane Shock Produced by Hypervelocity Impact and Late-Stage Equivalence", Journal of Applied Physics, 37, p. 853-860, 1966
19. Chester, W., "The Quasi-Cylindrical Shock Tube", Phil. Maj. 7, 45, p. 1293-1301, 1954
20. Chisnell, R. F., "The Normal Motion of a Shock Wave Through a Non-Uniform One-Dimensional Medium", Proc. Roy. Soc. A-232, p. 350-370, 1955
21. Whitham, G. B., "On the Propagation of Shock Wave Through Regions of Non-Uniform Area on Flow", Journal of Fluid Mechanics, 4, p. 337-360, 1958
22. Collin, R. and M. Holt., "Intense Explosions at the Ocean Surface, " Physics of Fluid, 11, p. 701-713, 1968

23. Walsh, J. M., W. E. Johnson, J. K. Dienes, J. H. Tillotsen, and D. R. Yates, "Summary Report on the Theory of Hypervelocity Impact", Gordon and Breach Science Publishers, 1964
24. Rayzer, Yu. P., "Motion of a Gas Under the Influence of a Point-Impact Shock on Its Surface (An Explosion on a Surface)", Zhurnal Prikladnoi Mekhunki A. Tekhnickiski Fiziki, No. 1, pp. 57-66, 1963. Translation, by M. J. Nowak, available as General Atomic Division, General Dynamics Corp., Report No. GA-tr-5081, May 1964
25. Skews, B. W., "The Shape of a Diffracting Shock Wave", Journal of Fluid Mechanics, 29, p. 297-304, 1967
26. Heyda, J. F. and T. D. Riney, "Penetration of Structures by Hypervelocity Projectiles", General Electric Company, Space Sciences Laboratory, Report No. R64SD3, February 1964
27. Riney, T. D. and J. F. Heyda, "Theoretical Prediction of Crater Size for Hypervelocity Impact by Reduced-Density Particles", General Electric Company, Final Report under Contract NADA 3-5812, February, 1968
28. Duvall, G. E., "Concepts of Shock Wave Propagation", Bulletin of the Seismological Society of America, Vol. 52, No. 4, p. 869-893, October 1962